AEDC-TR-79-36

$o_{4}.I$

$3\ 9\ c^{.0}$

AN ACOUSTIC SOURCE MODELING TECHNIQUE
TO PREDICT THE NEAR SOUND FIELD OF
AXISYMMETRIC TURBULENT JETS

J. R. Maus, C. V. Sundaram,
L. B. Bates, and M. G. Scott

THE UNIVERSITY OF TENNESSEE SPACE INSTITUTE
TULLAHOMA, TENNESSEE 37388

May 1979

Final Report for Period September 1, 1977 — November 15, 1978

Prepared for

ARNOLD ENGINEERING DEVELOPMENT CENTER/DOTR
ARNOLD AIR FORCE STATION, TENNESSEE 37389

This final report was submitted by The University of Tennessee Space Institute, Tullahoma, Tennessee 37388, under Contract F40600-77-C-0009 with the Arnold Engineering Development Center/DOTR, Air Force Systems Command, Arnold Air Force Station, Tennessee 37389. Mr. Eules L. Hively, DOTR, was the Air Force Project Manager.

This report has been reviewed by the Information Office (OI) and is releasable to the National Technical Information Service (NTIS). At NTIS, it will be available to the general public, including foreign nations.

APPROVAL STATEMENT

This report has been reviewed and approved.

EULES L. HIVELY
Project Manager, Research Division
Directorate of Test Engineering

Approved for publication:

FOR THE COMMANDER

ROBERT W. CROSSLEY, Lt Colonel, USAF
Acting Director of Test Engineering
Deputy for Operations

UNCLASSIFIED

REPORT DOCUMENTATION PAGE		READ INSTRUCTIONS BEFORE COMPLETING FORM
1 REPORT NUMBER AEDC-TR-79-36	2 GOVT ACCESSION NO.	3. RECIPIENT'S CATALOG NUMBER
4 TITLE (and Subtitle) AN ACOUSTIC SOURCE MODELING TECHNIQUE TO PREDICT THE NEAR SOUND FIELD OF AXISYMMETRIC TURBULENT JETS		5 TYPE OF REPORT & PERIOD COVERED Final Report - Sep 1, 1977 - Nov 15, 1978
		6 PERFORMING ORG. REPORT NUMBER
7 AUTHOR(s) J. R. Maus, C. V. Sundaram, L. B. Bates, and M. G. Scott		8 CONTRACT OR GRANT NUMBER(s) F40600-77-C-0009
9 PERFORMING ORGANIZATION NAME AND ADDRESS The University of Tennessee Space Institute, Tullahoma, Tennessee 37388		10. PROGRAM ELEMENT, PROJECT, TASK AREA & WORK UNIT NUMBERS Program Element 65807F
11 CONTROLLING OFFICE NAME AND ADDRESS Arnold Engineering Development Center/OIS Air Force Systems Command Arnold Air Force Station, Tennessee 37389		12 REPORT DATE May 1979
		13 NUMBER OF PAGES 76
14 MONITORING AGENCY NAME & ADDRESS(if different from Controlling Office)		15 SECURITY CLASS. (of this report) UNCLASSIFIED
		15a DECLASSIFICATION/DOWNGRADING SCHEDULE N/A

16 DISTRIBUTION STATEMENT (of this Report)

Approved for public release; distribution unlimited.

17 DISTRIBUTION STATEMENT (of the abstract entered in Block 20, if different from Report)

18 SUPPLEMENTARY NOTES

Available in DDC

19 KEY WORDS (Continue on reverse side if necessary and identify by block number)

sound waves	models
sound pressure	engines
jets	test facilities
turbulent flow	acoustic measurement

20. ABSTRACT (Continue on reverse side if necessary and identify by block number)

The objective of the investigation reported herein was to develop a technique for determining the free, unreflected sound field produced by a jet engine based on sound measurements obtained in an engine test cell. As a first step in this direction, a procedure has been developed for modeling the sound sources in an axisymmetric jet which allows prediction of the near sound field

DD FORM 1473 EDITION OF 1 NOV 65 IS OBSOLETE
1 JAN 73

UNCLASSIFIED

20. ABSTRACT   (Continued)

generated by the jet.   The procedure involves modeling the sources
for each one-third octave frequency band by a combination of un-
correlated elementary sources derived from the multipole expansion.
The strengths of the various source components at a particular
frequency are determined by a constrained least squares fit to the
far field directivity pattern.   When the effects of source motion
and axial source distribution with frequency are taken into
account, the computed sound field agrees reasonably well with data
obtained in the near field.   The results of the study indicate,
however, that it will be very difficult to predict the far field
sound from acoustic measurements in an engine test cell.

AFSC
Arnold AFS Tenn

PREFACE

The work reported herein was conducted by The University of Tennessee Space Institute between September 1977 and November 1978. The work was sponsored by the Arnold Engineering Development Center (AEDC), Air Force Systems Command (AFSC), under Contract F40600-77-C-0009. The Air Force Program Manager for the contract was Mr. Eules L. Hively.

The study was suggested by Dr. M. L. Laster and Dr. B. H. Goethert. Mr. James R. Goodman assisted in all experimental phases of the investigation, and discussions with Dr. William A. Dunnill were very helpful in developing the analytic formulation. The authors express their sincere appreciation to these individuals.

The reproducibles used in the reproduction of this report were supplied by the authors.

CONTENTS

LIST OF FIGURES

I. INTRODUCTION

The acoustic environment of an engine test cell of the type at the Engine Test Facility of AEDC is extremely complex. The sound field present in such a cell consists of a direct component, due to the sound pressure waves emanating directly from the distributed source, and a reverberant field associated with waves reflected from the surfaces of the enclosure. The relative contribution of these two components must be determined in order to either model the acoustic field in the test cell or infer the strength and nature of sources from in-cell measurements to predict the free field sound that such sources would produce.

One factor that affects the relative contribution of the direct and indirect fields is the strength of the near field component of the direct radiation field. It is well known that the sound pressure near an acoustic source can vary much more strongly than the $1/r$ relation that applies in the far field. In this region the sound pressure is not in phase with the acoustic particle velocity and cannot be directly related to acoustic energy flux. Thus, one of the problems that must be addressed before substantial progress can be made toward an understanding of the acoustic environment in an engine test cell is that of interpreting near field acoustic data and their relation to the acoustic sources and far field sound.

The primary objective of the present study is to determine the relationship between acoustic measurements in the near field and the far field sound produced by a free circular jet. A longer range objective of the research effort is to attempt to establish techniques for predicting the far sound field using in-cell acoustic measurements.

The sound source used throughout this study was a free turbulent jet exhausting from a convergent circular nozzle. In the engine test cells at AEDC, the exhaust jet from the engine is captured by a scavenging duct or diffuser. The inlet of this duct is normally located a very short distance downstream of the engine exhaust nozzle. In this investigation no attempt was made to take into account the effects of the scavenger duct of the surrounding test section walls.

The general approach taken in this study was to model the jet source region, for a given frequency, with a combination of uncorrelated elementary sources derived from the multipole expansion. The strengths of the various source components at a particular frequency were determined from measured 1/3 octave far field directivity patterns. Initially, it was assumed that the jet noise source distribution could be replaced by an equivalent stationary source distribution which could be approximated by a group of elementary sources centered in the nozzle exit plane. During the course of the investigation, it was found that in order to closely approximate the near acoustic field, it was necessary to introduce the motion of the sources and their distribution along the jet axis with frequency.

7

II. STATIONARY SOURCE MODEL

In this section equations are developed for synthesizing the source region for an axisymmetric turbulent jet, assuming that the true noise sources can be replaced by an equivalent stationary source distribution.

2.1   MULTIPOLE EXPANSION

The sound pressure field produced by a stationary distributed source $f(x_1, x_2, x_3, t)$ is governed by the non-homogeneous wave equation

$$\frac{\partial^2 p}{\partial x_1^2} + \frac{\partial^2 p}{\partial x_2^2} + \frac{\partial^2 p}{\partial x_3^2} - \frac{1}{a_o^2} \frac{\partial^2 p}{\partial t^2} = - f(x_1, x_2, x_3, t) \qquad (2.1)$$

In the absence of any reflecting walls the free-field solution to this equation is given by

$$p(\vec{x}, t) = \int_s \frac{f(\vec{y}, t - R/a_o)}{4\pi x} \, d\vec{y} \qquad (2.2)$$

where $\vec{x}$ is the position vector to the field point, $\vec{y}$ is the position vector to a source point and $R = |\vec{x} - \vec{y}|$. The geometry under consideration is illustrated in Fig. 1 showing the various position vectors. It is assumed that the distributed source is located in the neighborhood of the origin of the coordinate system.

The integral solution (2.2) is extremely difficult to evaluate even if the source function is known a priori. However, by expanding the integrand in a Taylor series about $\vec{x} = \vec{x}$, a series expression for the sound pressure field can be obtained which is frequently more tractable. (Ref. 1).

$$p(\vec{x}, t) = \sum_{jk\ell = 0}^{\infty} \frac{\partial^{j+k+\ell}}{\partial x_1^j \partial x_2^k \partial x_3^\ell} \frac{(-1)^{j+k+\ell}}{4\pi x} m_{jk\ell} \left(t - \frac{x}{a_o}\right) \qquad (2.3)$$

This series is called a multipole expansion and functions $m_{jk\ell}(t)$ are called

multipole moments of the source distribution:

$$m_{jk\ell}(t) = \int_s \frac{y_1^j \, y_2^k \, y_3^\ell}{j! \, k! \, \ell!} f(\vec{y}, t) \, dy \qquad (2.4)$$

The multipole expansion, in effect, replaces the distributed source by an infinite combination of elementary point sources located at the origin of the coordinate system. The leading term of Eq. 2.3 where $j = k = \ell = 0$ represents a monopole source with sound pressure field

$$P_m = \frac{1}{4\pi x} \, m_{000} \left(t - \frac{x}{a_0}\right) \tag{2.5}$$

The next three terms of the series with $j+k+\ell = 1$ correspond to dipole sources with sound pressure fields

$$P_{d_1} = -\frac{\partial}{\partial x_1} \left[\frac{m_{100}\left(t - \frac{x}{a_0}\right)}{4\pi x}\right]$$

$$P_{d_2} = -\frac{\partial}{\partial x_2} \left[\frac{m_{010}\left(t - \frac{x}{a_0}\right)}{4\pi x}\right] \tag{2.6}$$

$$P_{d_3} = -\frac{\partial}{\partial x_3} \left[\frac{m_{001}\left(t - \frac{x}{a_0}\right)}{4\pi x}\right]$$

The six terms corresponding to $j+k+\ell = 2$ are known as quadrupole terms and the ten terms with $j+k+\ell = 3$ are known as octupole terms. In general, terms with $j+k+\ell = n$ correspond to multipoles of order 2^n.

If it is assumed, for the moment, that all parts of source region are oscillating in phase, at a single frequency, the source function can be written as

$$f(\vec{y},t) = F(\vec{y}) \, e^{i\omega t} \tag{2.7}$$

and the multipole moments become

$$m_{jk\ell}(t) = M_{jk\ell} \, e^{i\omega t}$$

where

$$M_{jk\ell} = \int_s y_1^j \, y_2^k \, y_3^\ell \, F(\vec{y}) \, d\vec{y}$$

Introducing spherical polar coordinates as shown in Fig. 2 with

$$\frac{x_1}{x} = \cos\theta\sin\psi \qquad \frac{x_2}{x} = \sin\theta\sin\phi \qquad \frac{x_3}{x} = \cos\phi$$

the sound pressure fields for the monopole and dipole terms can be written as

$$p_m(\vec{x},t) = \frac{M_{000}}{4\pi x} e^{i(\omega t - \frac{x}{a_0})} \qquad (2.8)$$

$$p_{d_1}(\vec{x},t) = \frac{i\ k\ \sin\phi\cos\theta M_{100}}{4\pi x} (1 - \frac{i}{kx}) e^{i(\omega t - \frac{x}{a_0})}$$

$$p_{d_2}(\vec{x},t) = \frac{i\ k\ \sin\phi\sin\theta M_{010}}{4\pi x} (1 - \frac{i}{kx}) e^{i(\omega t - \frac{x}{a_0})} \qquad (2.9)$$

$$p_{d_3}(\vec{x},t) = \frac{i\ k\ \cos\phi\ M_{001}}{4\pi x} (1 - \frac{i}{kx}) e^{i(\omega t - \frac{x}{a_0})}$$

where $k = \frac{\omega}{a_0} = \frac{2\pi}{\lambda}$ is called the wave number.

It should be noted that the factor $(1 - i/kx)$ in Eq. 2.9 contains the near field contribution for the dipole sound pressure. As $kx = 2\pi x/\lambda$ becomes much larger than unity, so that the observer is many wave lengths from the source, this factor approaches one, resulting in the far field expression for the dipole sound pressure. Equations for the quadrupole and octupole contributions to the sound field, similar to Eq. 2.9, have been derived but these are much more lengthy and are therefore not presented in the body of this report. A full listing of the equations used in computing the near and far sound fields is presented in Appendix A.

2.2   COMBINATION OF UNCORRELATED SOURCES

Considering the source region as the axi-symmetric turbulent jet flow from a circular nozzle, the sound field produced by this source distribution should possess axial symmetry. As will be shown, however, care must be taken as to how this symmetry condition is introduced. If, for example, the source function given in Eq. 2.7 is assumed to be symmetric about the x_3 axis, the axis of the jet, it takes the form

$$f(\vec{y},t) = F(r,y_3)e^{i\omega t} \qquad (2.10)$$

where
$$r^2 = y_1^2 + y_2^2$$

If such a source distribution is used, many of the multipole moments vanish identically. In particular, the dipole moments M_{100} and M_{010} are zero and the dipole contribution to the sound pressure field becomes

$$P_d = \frac{i \ k \ \cos\phi M_{001}}{4\pi x} \ (1 - \frac{1}{kx}) \ e^{i(\omega t - \frac{x}{a_o})}$$

This pressure field would be added to that for the monopole and surviving higher order poles to produce a sound field that is axially symmetric.

Further reflection, however, reveals that the assumptions made in writing Eq. 2.9 are much too restrictive. At a particular frequency, both the source region and the sound field produced would be axially symmetric on an instantaneous basis with respect to amplitude and phase. The acoustic sources in a jet flow are directly related to flow turbulence and are therefore random in nature. Thus while the acoustic source distribution at a particular frequency may be regarded as axi-symmetric with respect to average amplitude, it is certainly not symmetric on an instantaneous basis as was assumed in Eq. 2.9.

A second method that appears more realistic is to model the source with an assemblage of uncorrelated elementary sources (monopole, dipole, etc.) These sources can be combined in such a way as to produce a sound field that is axisymmetric with respect to mean square pressure. This technique has been used by Mani et. al. (Ref. 2) to model the source distribution for a small circular jet in an open jet wind tunnel.

To illustrate this approach, consider the contribution to the sound field due to dipole radiation. If it is assumed that the three dipoles given by Eqs. 2.8 are uncorrelated, the mean squares of the acoustic pressures add to give the mean square pressure due to dipole radiation:

$$\overline{p_d^2} = \overline{p_{d_1}^2} + \overline{p_{d_2}^2} + \overline{p_{d_3}^2}$$

$$= \frac{k^2}{(4\pi x)^2} \left[1 + \frac{1}{(kx)^2} \right] (M_{100}^2 \sin^2\phi \cos^2\theta + M_{010}^2 \sin^2\phi \sin^2\theta + M_{001}^2 \cos^2\phi) \tag{2.11}$$

The sound field given by this equation is not symmetric about the jet axis for arbitrary values of the dipole moments. However, if the strengths of the x_1 and x_2 dipoles are the same so that $M_{100} = M_{010}$, the dependence on azimuthal angle θ disappears yielding

$$\overline{p_d^2} = \frac{k^2}{(4\pi x)^2} \left[1 + \frac{1}{(kx)^2}\right] (M_{100}^2 \sin^2 \phi + M_{001}^2 \cos^2 \phi) \qquad (2.12)$$

This is the most general form for a combination of uncorrelated dipoles that produces an axially symmetric sound field. In the acoustic far field, where $kx \gg 1$, Eq. 2.12 reduces to

$$\overline{p_d^2} = \frac{k^2}{(4\pi x)^2} (M_{100}^2 \sin^2 \phi + M_{001}^2 \cos^2 \phi) \qquad (2.13)$$

Equations similar to Eq. 2.12 for the mean square sound pressure for uncorrelated quadrupoles and octupoles are given in Appendix A. The far field approximations for the mean square sound pressure for monopole, dipole, quadrupole, and octupole sources are shown below.

$$\overline{p_m^2} = \frac{M_{000}^2}{(4\pi x)^2}$$

$$\overline{p_d^2} = \frac{k^2}{(4\pi x)^2} [M_{100}^2 \sin^2 \phi + M_{001}^2 \cos^2 \phi]$$

$$(2.14)$$

$$\overline{p_q^2} = \frac{k^4}{(4\pi x)^2} [M_{200}^2 \sin^4 \phi + M_{110}^2 \sin^2 \phi \cos^2 \phi + M_{002}^2 \cos^4 \phi]$$

$$\overline{p_o^2} = \frac{k^6}{(4\pi x)^2} [M_{030}^2 \sin^6 \phi + M_{021}^2 \sin^4 \phi \cos^2 \phi + M_{012}^2 \sin^2 \phi \cos^4 \phi + M_{003}^2 \cos^6 \phi]$$

The total mean square pressure is obtained by combining the contributions of the above sources, assuming that they are uncorrelated. Thus,

$$\overline{p^2} = \overline{p_m^2} + \overline{p_d^2} + \overline{p_q^2} + \overline{p_o^2} \qquad (2.15)$$

2.3 UNIQUENESS CONDITION

In order to complete the synthesis of the acoustic sources, the multipole moments M^2_{000}, M^2_{100}, M^2_{001}, etc., must be determined for a given frequency. This was done by using a least squares technique to determine the constants that best fit the far field sound pressure data at a particular frequency. The multipole moments, however, are not uniquely determined by this procedure. To illustrate this, suppose the far field sound at some frequency is accurately represented by the combination of a monopole and two dipoles. Then

$$\overline{p^2} = \frac{M^2_{000}}{(4\pi x)^2} + \frac{k^2}{(4\pi x)^2} [M^2_{100} \sin^2 \phi + M^2_{001} \cos^2 \phi] \tag{2.16}$$

By using the identity $\sin^2\phi + \cos^2\phi = 1$, Eq. 2.16 can be rewritten as

$$\overline{p^2} = \frac{k^2}{(4\pi x)^2} [M^{*2}_{100} \sin^2 \phi + M^{*2}_{001} \cos^2 \phi] \tag{2.17}$$

where

$$M^{*2}_{100} = M^2_{100} + \frac{M^2_{000}}{k^2}$$

$$M^{*2}_{001} = M^2_{001} + \frac{M^2_{000}}{k^2}$$

Similarly, if $M^2_{001} > M^2_{100}$, the mean square pressure can be written as

$$\overline{p^2} = \frac{M'^2_{000}}{(4\pi x)^2} + \frac{k^2}{(4\pi x)^2} M'^2_{001} \cos^2 \phi \tag{2.18}$$

where

$$M'^2_{001} = M^2_{001} - M^2_{100}$$

$$M'^2_{000} = M^2_{000} + k^2 M^2_{100}$$

While these three expressions give the same sound pressure in the far field, the near field pressures are not the same, because the near field terms are different for a monopole and a dipole.

13

In order to uniquely determine the multipole moments, an additional condition suggested by Mani (Ref. 2) is imposed based on the intuitive concept that the lower order sources should have their maximum possible strength. Using this condition in the example above specifies Eq. 2.18, since M'_{000} is the largest possible monopole moment.

As a further example of the application of this uniqueness condition, suppose that the far field sound is accurately expressed in terms of a combination of uncorrelated quadrupoles. Then

$$\overline{p^2} = Q_1 \sin^4 \phi + Q_2 \sin^2 \phi \cos^2 \phi + Q_3 \cos^4 \phi \tag{2.19}$$

where

$$Q_1 = \frac{k^4 M_{200}}{(4\pi x)^2} \quad , \quad Q_2 = \frac{k^4 M_{110}}{(4\pi x)^2} \, , \quad Q_3 = \frac{k^4 M_{002}}{(4\pi x)^2}$$

The identity $\sin^4 \phi + 2 \sin^2 \phi \cos^2 \phi + \cos^4 \phi = 1$ can be used to extract the largest embedded monopole. Let

$$P_1 = \min (Q_1, \, Q_2/2, \, Q_3) = \frac{M_{000}^2}{4\pi x}$$

and redefine

$$Q'_1 = Q_1 - P_1, \quad Q'_2 = Q_2 - 2P_1, \quad Q'_3 = Q_3 - P_1$$

Then Eq. 2.19 becomes

$$\overline{p^2} = P_1 + Q'_1 \sin^4 \phi + Q'_2 \sin^2 \phi \cos^2 \phi + Q'_3 \cos^4 \phi \tag{2.20}$$

Next use the identity $\sin^2 \phi + \cos^2 \phi = 1$ to remove the embedded dipoles. Let

$$D_1 = \min (Q'_1, \, Q'_2) = \frac{k^2 M_{100}^2}{(4\pi x)^2}$$

and redefine

$$Q''_1 = Q'_1 - D_1, \quad Q''_2 = Q'_2 - D_1, \quad Q''_3 = Q'_3$$

Similarly let

$$D_2 = \min(Q_1'', Q_2'') = \frac{k^2 M^2{}_{001}}{(4\pi x)^2}$$

and redefine

$$Q_1''' = Q_1'', \quad Q_2''' = Q_2'' - D_2, \quad Q_3''' = Q_2'' - D_2$$

This gives the desired representation for the sound pressure field with the lower order sources having their maximum strength

$$\overline{p^2} = P_1 + D_1 \sin^2\phi + D_2 \cos^2\phi + $$

$$Q_1''' \sin^4\phi + Q_2''' \sin^2\phi\cos^2\phi + Q_3''' \cos^4\phi \qquad (2.21)$$

This procedure is easily extended to any level of the multipole expansion. In the present study the expansion was truncated at the octupole level, so that a least squares fit was used to determine constants

$$A_1 = \frac{k^6 M^2{}_{030}}{(4\pi x)^2}, \qquad\qquad A_2 = \frac{k^6 M^2{}_{021}}{(4\pi x)^2},$$

$$A_3 = \frac{k^6 M^2{}_{012}}{(4\pi x)^2}, \qquad\qquad A_4 = \frac{k^6 M^2{}_{003}}{(4\pi x)^2}$$

in the equation.

$$p^2 = A_1 \sin^6\phi + A_2 \sin^4\phi\cos^2\phi + A_3 \sin^2\phi\cos^4\phi$$

$$+ A_4 \cos^6\phi \qquad (2.22)$$

15

The identities

$$\sin^6\phi + 3\sin^4\phi\cos^2\phi + 3\sin^2\phi\cos^4\phi + \cos^6\phi = 1$$

$$\sin^4\phi + 2\sin^2\phi\cos^2\phi + \cos^6\phi = 1$$

$$\sin^2\phi + \cos^2\phi = 1$$

were used to extract the embedded monopole, dipoles, and quadrupoles using the procedure discussed above.

2.4   CONSTRAINED LEAST SQUARES FIT

It should be noted that the constants, A_1, A_2, A_3, A_4 in Eq. 2.22 must all be non-negative according to the derivation. Consequently, a simple least squares procedure cannot be used to determine these quantities. In (Ref. 3), a constrained least squares algorithm based on the Kuhn Tucker Theorem is presented. A Fortran subroutine based on this algorithm was adapted to the present problem to determine values of A_1, A_2, A_3, A_4, that best fit the measured sound pressure data subject to the constraint $A_1 \geq 0$.

III. EXPERIMENTAL PROGRAM

3.1 EXPERIMENTAL FACILITIES

All acoustic data obtained in this study were gathered in the UTSI free field facility shown in Fig. 3. This facility has been described in detail in Ref. 4 and only the essential features will be discussed here. The test facility was basically designed to be used to investigate the sound field generated by high velocity turbulent air jets. The air supply system for the test rig is capable of delivering air mass flows in excess of 40 lb$_m$/sec at stagnation temperatures up to 1000°F. Being a blow-down facility, the run time is inversely proportional to the air mass flow rate, with a flow of 40 lb$_m$/sec corresponding to about a 3 minute run.

Acoustic data on air jets are normally taken with the stilling chamber and exhaust jet axis oriented at an angle of about 35 1/2° to the ground plane, as shown in Fig. 3. It is convenient to introduce a coordinate system with origin in the center of the nozzle exit plane and with the x_3 axis coincident with the exhaust jet axis. This is consistent with the notation of Section II. Sound pressure data can be taken with either of two microphone sweep arms: a rear arm sweeping in the nozzle exit x_1,x_2 plane and a side arm sweeping in a plane containing the jet axis, the x_1,x_3 plane. For normal operation, the microphones mounted on the arms are at a constant distance of 13 feet from the center of the nozzle exit plane during a sweep. At this distance, the microphones are in the far field for all frequencies greater than about 100 Hz. The sweep arms are adjustable, so that the distance from the microphone to the nozzle center can be varied over a wide range. In particular, the side arm can be adjusted to sweep the microphone in the x_1,x_3 plane at about one foot from the coordinate system origin. This feature was used in obtaining near field data in the present study.

3.2 ACOUSTIC DATA

All acoustic test data in the present study were taken on high velocity jets exhausting from a converging circular nozzle with a 2.82 inch exit diameter. In order to avoid noise sources associated with shocks in the flow, the exit Mach number of the jet exhaust was kept below one. Four different combinations of stagnation pressures and temperatures were used in order to vary the jet exit velocity, and consequently, sound source power over a wide range. The flow conditions used in this study are given in the table below.

TABLE 1. TEST CONDITIONS

Condition No.	P_o/P_a	Mach No.	T_o,°R	Velocity ft/sec
1	1.387	0.7	540	755
2	1.691	0.9	530	943
3	1.691	0.9	1160	1396
4	1.787	0.95	1260	1524

For each of the conditions shown in Table 1, a series of acoustic data were obtained. Far field data in the x_1,x_3 plane were taken first with the microphone located 13 ft from the origin of the coordinate system. One third octave sound pressure spectra were obtained at 5 degree increments of polar angle, ϕ, starting at $\phi = 20°$ to $\phi = 90°$. The polar angle, ϕ, as shown in Fig. 2, is measured from the x_3 axis, the axis of the exhaust jet. Figs. 4, 5, and 6 are examples of these far field spectra measured for Test Condition 3. From spectrograms such as these, the 1/3 octave far field directivity patterns were plotted for center frequencies of 100, 200, 500, 1000, 2000, 5000, and 10,000 Hz. Figs. 7, 8, and 9 are examples of the far field directivites for Test Condition 3. It should be noted that the 1/3 octave frequency analysis is a constant percentage analysis with the filter bandwidths equal to 23 percent of the center frequency. Thus, the frequency bandwidth of the 100 Hz data in Fig. 7 is 23 Hz and the bandwidth of the 1000 Hz data in Fig. 8 is 230 Hz. Data such as shown in Figs. 7, 8, and 9 were used to obtain the strengths of the uncorrelated elementary sources, as described in Section II.

Near field data for the test conditions listed in Table 3 were obtained by readjusting the side sweep arm to bring the microphone closer to the center of the nozzle exit plane. Data were obtained in the x_1,x_3 plane for radial distances between 1 ft and 4 ft at approximately 1 ft intervals. At each radial distance, 1/3 octave spectra were taken at several angular positions so the radial variation of sound pressure could be plotted for different frequencies and angular orientations. Figs. 10, 11, and 12 are examples of these data for Test Condition 3. The straight solid lines in these figures corresponds to a far field variation of $p \propto 1/r^2$.

IV.   RESULTS OF STATIONARY SOURCE MODEL

In this section a comparison of the results of the stationary source model with the acoustic data obtained in the experimental program are presented.   The first group of comparisons in Figs. 13 through 15 illustrate the degree to which the far field directivity patterns can be represented by a combination of uncorrelated singularities through the octupole level.   The curves in these figures were obtained from the equation

$$\overline{p^2} = A_1' \sin^6 \phi + A_2' \sin^4 \phi \cos^2 \phi + A_3' \sin^2 \phi \cos^4 \phi + A_4' \cos^6 \phi$$

where A_1', A_2', A_3', A_4' are four positive constants selected to give the best fit in least squares sense to the experimental directivity pattern.   The acoustic pressures in these and all other figures in this report are given as Sound Pressure Levels in a decibel scale.

$$SPL = 10 \log_{10} \frac{\overline{p^2}}{p^2_{ref}} \text{, dB}$$

where

$$P_{ref} = 2 \times 10^{-5} \text{ N/m}^2.$$

Using the procedure described in Section II, the moments of the largest embedded monopole, P_1, was determined as

$$P_1 = \min (A_1', A_2'/3, A_3'/3, A_4').$$

The dipole moments D_1, D_2, the quadrupole moments Q_1, Q_2, Q_3, and the reduced octupole moments A_1, A_2, A_3, A_4 were obtained as described in Section II. These values are given in the legends of Figs. 13 through 15.

These results, and others similar to them, show that the multipole expansion for a stationary source distribution gives a good representation of the far field directivity produced by a circular jet.   Curves similar to those shown in Figs. 13 through 15 were obtained for the four test conditions given in Table 1 and for seven frequencies: 100, 200, 500, 1000, 2000, 5000, and 10,000 Hz.   For all test conditions and all frequencies considered, the discrepancy between the experimental data and the best fit for the multipole expansion was less than 4 dB.

A comparison of the radial distribution of sound pressure, as computed from the multipole expansion and measured in the experimental program, is

presented in Figs. 16 through 18. Using the coefficients listed in Figs. 13 through 15 in the full multipole expansion, including the near field terms, the sound pressure level was computed along rays emanating from the center of the nozzle exit plane. Examination of the results shown in Figs. 16 through 18 shows that the multipole expansion predicts the sound field reasonably well at high frequencies where the near field terms are of minor importance. As the frequency under consideration decreases and the near field terms in the multipole expansion become increasingly important, the measured and predicted sound pressure values near the jet exhaust diverge. The computed values of the sound pressure are in almost all cases greater than those measured. This trend suggests that the stationary source model is giving too large a near field contribution to the calculated sound field. Reference to Appendix A shows that importance of the near field terms increases with the order of the pole: the monopole has no near field; the near field terms of the dipole are proportional to $1/(kx)^2 = (\lambda/2\pi x)^2$; the quadrupole near field terms are of order $1/(kx)^4$; and the octupole terms are of order $1/(kx)^6$. Thus, the stationary source model is resulting in too great a contribution from the higher order poles. This, in turn, is due to the directionality of the far field sound distribution which can be adequately modeled only with the inclusion of these higher order terms.

Closer examination of the measured radial sound pressure distribution for low frequencies reveals that the mean square sound pressure drops off even more slowly than $\bar{p}^2 \propto 1/r^2$ predicted for the far field. This is perhaps best seen in Figs. 10 and 11 where the straight lines represent the far field relation. This discrepancy obviously cannot be overcome by the inclusion of near field terms, but must be accounted for in some other way.

In the next section, modifications of the stationary source model are introduced, which result in substantial improvement in the agreement with the experimental data.

V. MODIFICATION OF STATIONARY SOURCE MODEL

5.1 SOURCE CONVECTION EFFECTS

In the stationary source model presented in Section II, the multipole expansion was used as if sound source distribution were at rest with respect to the observer. In fact, the elementary sound sources are fluctuating turbulent eddies which are being convected by the mean flow with a convection velocity, V_c. This source motion tends to beam the sound field forward and produce a directionality that is not associated with the sources themselves. Thus, in the stationary source model, the source synthesis procedure is modeling an apparent source distribution rather than the true source distribution.

The jet noise theories of Lighthill (Ref. 5) and Ffowcs-Williams (Ref. 6) indicate that the far field sound intensity radiated from an axi-symmetric turbulent jet is given by

$$I(x,\phi) = \frac{\rho_m V_j^8 D^2}{\rho_o a_o^5 x^2} \cdot \frac{f(\phi)}{(1 - M_c \cos \phi)^5} \tag{5.1}$$

where x and ϕ are the polar coordinates of the far field observation point, ρ_m is a mean jet mixing region density, V_j is the jet exit velocity, and $M_c = V_c/a_o$ is a convection Mach number. The convection velocity, V_c, is less than the jet exit velocity and is thought to be frequency dependent. The factor $(1 - M_c \cos \phi)^{-5}$ takes into account the directionality of the sound field caused by the motion of the acoustic sources. The function $f(\theta)$ is associated with the inherent directionality of the source distribution. Considering the failure of the stationary source model to accurately predict the near field sound, it was decided to use the multipole expansion procedure to approximate the source directionality function $f(\theta)$.

To carry out the revised procedure, the measured far field intensities were divided by the convection factor $(1 - M_c \cos \theta)^{-5}$ prior to determination of the multipole moments. This removes the effect of source motion from the far field sound, so that the multipole expansion includes only the inherent directionality of the source region. This, in turn, reduces the weight of the higher order terms in the expansion with their strong near field components. The computed sound field from the source distribution is then multiplied by $(1 - M_c \cos \theta)^{-5}$ to obtain the predicted sound field. The unknown in this procedure is the ratio, R_c, of the convection velocity to the jet exit velocity. This ratio was adjusted at each frequency to remove as much angular variation from the sound field as possible.

Figs. 19 through 22 show some comparisons of far field sound directivity patterns from Test Condition 3 with the results of the multipole expansion after the convection effects have been removed. In general, a better fit to the data was obtained with the convection factor removed. The values of ratio R_c shown in the legends of these figures are not unreasonable.

5.2   EXTENDED SOURCE EFFECTS

In the stationary source model presented in Section II, for each frequency the distributed noise source of the turbulent jet was replaced by an assemblage of uncorrelated elementary sources located at the center of the nozzle exit plane. However, it is well known from jet noise theory (Ref. 7) that the location of the sound sources is frequency-dependent. The low frequency sound is generated by large scale turbulent eddies, which are located further downstream than the small scale sources of high frequency sound. In attempting to account for this effect, it was assumed that the effective source for each 1/3 octave frequency band can be considered as a point on the jet axis and that the location of the source is primarily a function of the Strouhal number, $St = f\, V_j/D$.

The initial investigation of this effect was performed by computationally varying the source location and determining the root mean square difference between the measured sound pressure level and that computed from the multipole expansion in the near field. The coefficients in the multipole expansion were determined from the far field measurements, after the convection effects had been removed as described above. A typical result of this computation is shown in Fig. 23. The approximate source location x_s is clearly revealed in this plot by the minimum error.

The approximate source locations, as determined by the above procedure for several frequencies and flow conditions, are plotted versus Strouhal Number in Fig. 24. The data exhibited in this graph show the expected trend that, as the frequency increases, the source location moves closer to the nozzle exit plane, $x_3 = 0$. The solid line in this figure was drawn by inspection to "best fit" the data and is given by

$$\frac{x_s}{D} = .7503\ (St)^{-.5624} \tag{5.2}$$

McGregor and Simcox (Ref. 8) have determined peak power source location data for flow from a circular nozzle by a wall isolation technique. Their results show the same general trend as that of Fig. 24, but locate the source somewhat farther downstream for a given Strouhal number.

5.3   RESULTS OF THE MODIFIED SOURCE MODELING PROCEDURE

Computations of the sound field for Test Conditions 1 through 4 were carried out using the modified source modeling procedure described above. The results of these calculations and a comparison with measured data are presented in Figs. 25 through 44. In performing these calculations, the coefficients in the multipole expansion were obtained from far field data at $x = 13$ ft, assuming a source location of $x_s = 0$. In all cases the multipole expansion was carried through the octupole terms and the convection effects were removed before evaluation of the multipole moments. In Figs. 25 through 44 all angles and distances are referred to a coordinate system fixed in the nozzle exit plane, as shown in Fig. 2, although the calculations using the equations of Section II were made with angles and distances based

on the source location for each frequency. No comparisons are presented for frequencies above 2000 Hz, since at higher frequencies the sources are located very near the nozzle exit and all microphone positions are in the far field.

In general, the predicted values agree reasonably well with the microphone data. However, fairly large discrepancies still occur for measurements very close to the nozzle and for small angles to the jet axis. The microphone measurements at 90° are those which are best described by the prediction scheme. This is, perhaps, to be expected, since in this direction the radiated sound is least affected by source convection or flow interaction effects.

VI. SUMMARY AND CONCLUSIONS

At the outset of this investigation, it had been hoped that the acoustic field produced by a free circular jet could be well modeled by a stationary distributed source, which could in turn be closely approximated by a multipole expansion centered at the origin of the coordinate system. It turned out that this approach produced a near field contribution much larger than obtained by actual measurements. In order to achieve better agreement with the experimental results, it was necessary to use a more realistic model for the source region. In particular, the fact that the acoustic sources in a jet flow are moving, being convected by the mean flow, had to be taken into account. Also, the fact that the low frequency noise sources are located further downstream from the nozzle exit plane than the high frequency sources had to be incorporated into the jet noise source model. With these modifications, calculations of the near acoustic field were carried out. A direct comparison of the calculated and measured sound field was presented in Section V and justify the following conclusion: The near and far acoustic fields produced by a circular jet can be reasonably well calculated, using a model source region consisting of uncorrelated elementary sources if the effects of source motion and distribution with frequency are taken into account.

A second conclusion reached on the basis of this investigation is that predicting free field acoustic data from measurements in the test cell will be very difficult. This conclusion is in part based on the fact that there appears to be no very strong direct near field contribution that is simply related to the far acoustic field. This being the case, it will be very difficult to separate the direct radiation field from the reverberant field caused by reflections from the test section wall.

A further complication in the test cell is the fact that the engine exhaust is captured by a diffuser or scavenger duct a short distance downstream of the nozzle exit. Thus, much of the sound generated by the exhaust jet may not be escaping into the test cell. On the other hand, if the nozzle exhaust impinges or scrubs the diffuser, additional noise sources will be present. There can be no doubt that the sound field produced by the exhaust jet – diffuser combination is quite different from that produced by the jet alone.

It is thought that a better understanding of the acoustic characteristics of the test cell and an investigation of the effect of the diffuser on the jet sound field must precede further efforts to predict far field acoustic data from measurements in the test cell. A study of these factors would also be of considerable value in any effort to predict or assess the acoustic environment in a test cell. For these reasons it is recommended that Phase II of the present contract be directed toward a detailed investigation of the acoustic field produced by the interaction of the jet exhaust with the scavenger duct and an attempt to theoretically describe the sound field within a test cell.

LIST OF REFERENCES

1. Goldstein, M. E., Aeroacoustics, McGraw Hill, 1976.

2. Mani, R., et. al, "Development of a Technique for Inflight Jet Noise Simulation - Part II." AIAA Paper No. 76-532, 1976.

3. Lawson, C. L. and R. J. Hanson, Solving Least Squares Problems, Prentice-Hall, 1974.

4. Goethert, B. H., et al., "Investigation of Feasible Nozzle Configurations for Noise Reduction in Turbofan and Turbojet Aircraft, Report No. FAA-RD-75-162-I, 1975.

5. Lighthill, M. J., "On Sound Generated Aerodynamically. I. General Theory" Proc. Roy. Soc. (London) Vol. 222A p. 1-32, 1954.

6. Ffowcs Williams, J. E. "The Noise from Turbulence Convected at High Speed," Phil. Trans. Roy Soc. Vol A225 p. 469-503, 1963.

7. Ribner, H. S., "The Generation of Sound by Turbulent Jets", Advances in Applied Mechanics, Vol. 8, p. 104-182, Academic Press, 1964.

8. McGregor, G. R. and C. D. Simcox, "Location of Acoustic Sources in Jet Flows by Means of Wall Isolation Technique." AIAA Paper 73-1041, 1973.

APPENDIX A

The mean square acoustic pressures associated with the monopole, dipole, quadruopole and octupole type sources are given below:

Monopole:

$$\overline{p^2}_m = \frac{M^2_{000}}{(4\pi x)^2} \qquad \text{(no nearfield terms)}$$

Dipole:

$$\overline{p^2}_d = \frac{k^2}{(4\pi x)^2} \left[1 + \frac{1}{(kx)^2}\right] (M^2_{100} \sin^2 \phi + M^2_{001} \cos^2 \phi)$$

Quadrupole:

$$\overline{p_q^2} = \frac{k^4 M^2_{200}}{(4\pi x)^2} [\sin^4 \phi + \frac{1}{(kx)^2} (3 \sin^4 \phi - 4 \sin^2 \phi + 2)$$

$$+ \frac{1}{(kx)^4} (9 \sin^4 \phi - 6 \sin^2 \phi + 2)]$$

$$+ \frac{k^4 M^2_{002}}{(4\pi x)^2} [\cos^4 \phi + \frac{1}{(kx)^2} (3 \cos^4 \phi - 4 \cos^2 \phi + 1)$$

$$+ \frac{1}{(kx)^4} (9 \cos^4 \phi - 6 \cos \phi + 1)$$

$$+ \frac{k^4 M^2_{101}}{(4\pi x)^2} \sin^2 \phi \cos^2 \phi [1 + \frac{3}{(kx)^2} + \frac{9}{(kx)^4}]$$

27

Octupole:

$$\overline{p^2}_0 = \frac{k^6 M^2_{300}}{(4\pi x)^2} \left[\sin^6 \phi + \frac{6}{(kx)^2} (\sin^6 \phi - 3 \sin^4 \phi + 2 \sin^2 \phi) \right.$$

$$+ \frac{1}{(kx)^4} (\sin^6 \phi - 72 \sin^4 \phi + 36 \sin^2 \phi)$$

$$+ \frac{1}{(kx)^6} (225 \sin^6 \phi - 270 \sin^4 \phi + 108 \sin^2 \phi)$$

$$+ \frac{k^6 M^2_{003}}{(4\pi x)^2} \left[\cos^6 \phi + \frac{3}{(kx)^2} (2 \cos^6 \phi - 6 \cos^4 \phi + 3 \cos^2 \phi) \right.$$

$$+ \frac{9}{(kx)^4} (5 \cos^6 \phi - 8 \cos^4 \phi + 3 \cos^2 \phi)$$

$$+ \frac{1}{(kx)^6} (225 \cos^6 \phi - 270 \cos^4 \phi + 81 \cos^2 \phi)$$

$$+ \frac{k^6 M^2_{021}}{(4\pi x)^2} \left[\sin^4 \phi \cos^2 \phi + \frac{6 \cos^2 \phi}{(kx)^2} (\sin^4 \phi - \sin^2 \phi + 2) \right.$$

$$+ \frac{3 \cos^2 \phi}{(kx)^4} (15 \sin^4 \phi - 8 \sin^2 \phi + 2)$$

$$+ \frac{9 \cos^2 \phi}{(kx)^6} (25 \sin^4 \phi - 10 \sin^2 \phi + 2)$$

$$+ \frac{k^6 M^2_{102}}{(4\pi x)^2} \left[\cos^4 \phi \sin^2 \phi + \frac{\sin^2 \phi}{(kx)^2} (6 \cos^4 \phi - 6 \cos^2 \phi + 1) \right.$$

$$+ \frac{3 \sin^2 \phi}{(kx)^4} (15 \cos^4 \phi - 8 \cos^2 \phi + 1)$$

$$+ \frac{9 \sin^2 \phi}{(kx)^4} (25 \cos^4 \phi - 10 \cos^2 \phi + 1) \right]$$

APPENDIX B

Figures
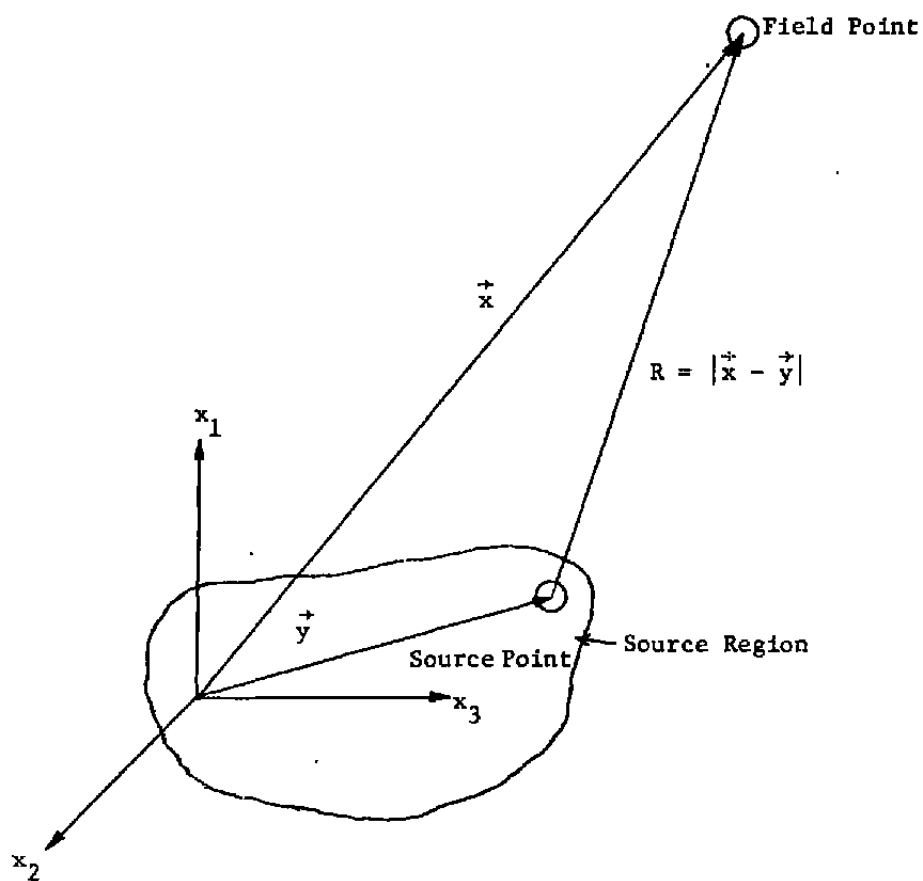
Fig. 1. Definition of Position Vectors for Stationary Source Model.
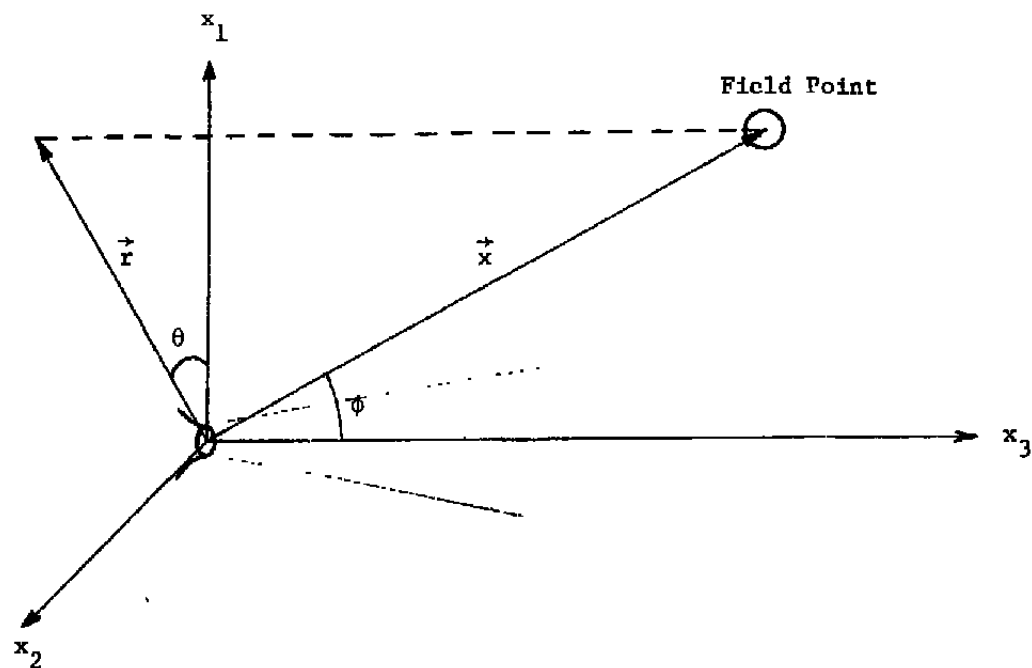
Fig. 2. Definition of Rectangular and Polar Coordinates for Stationary Source Model.

Microphones

Sweep
Arm

x_1, x_2

x_3

Nozzle
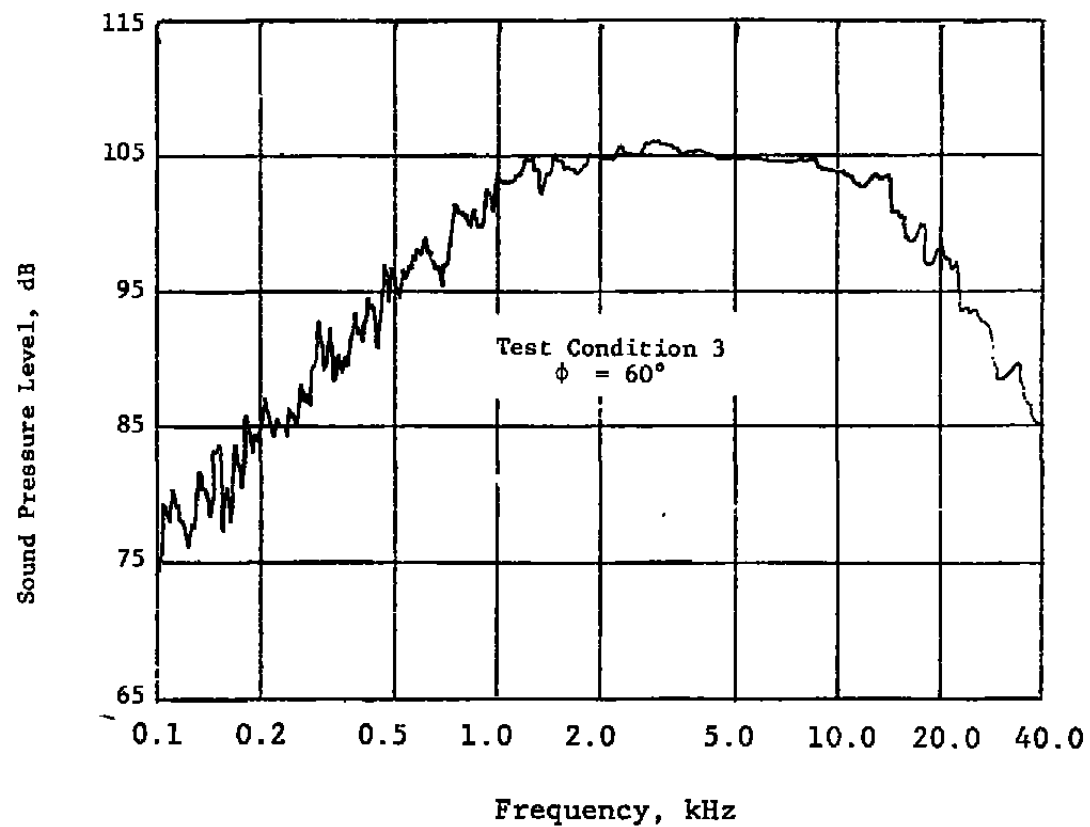
Stilling
Chamber
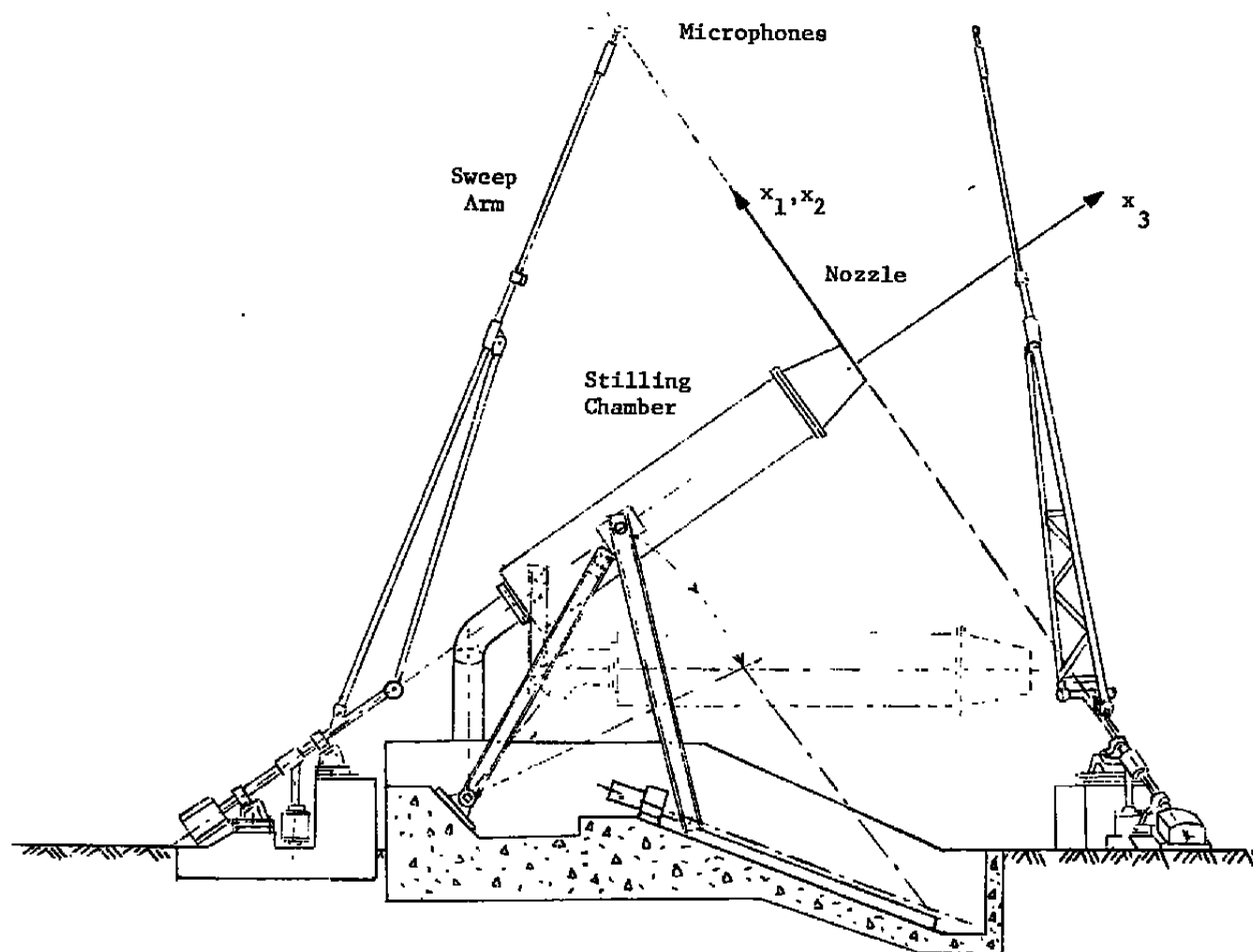
Fig. 3. Elevation View of Free Field Facility.
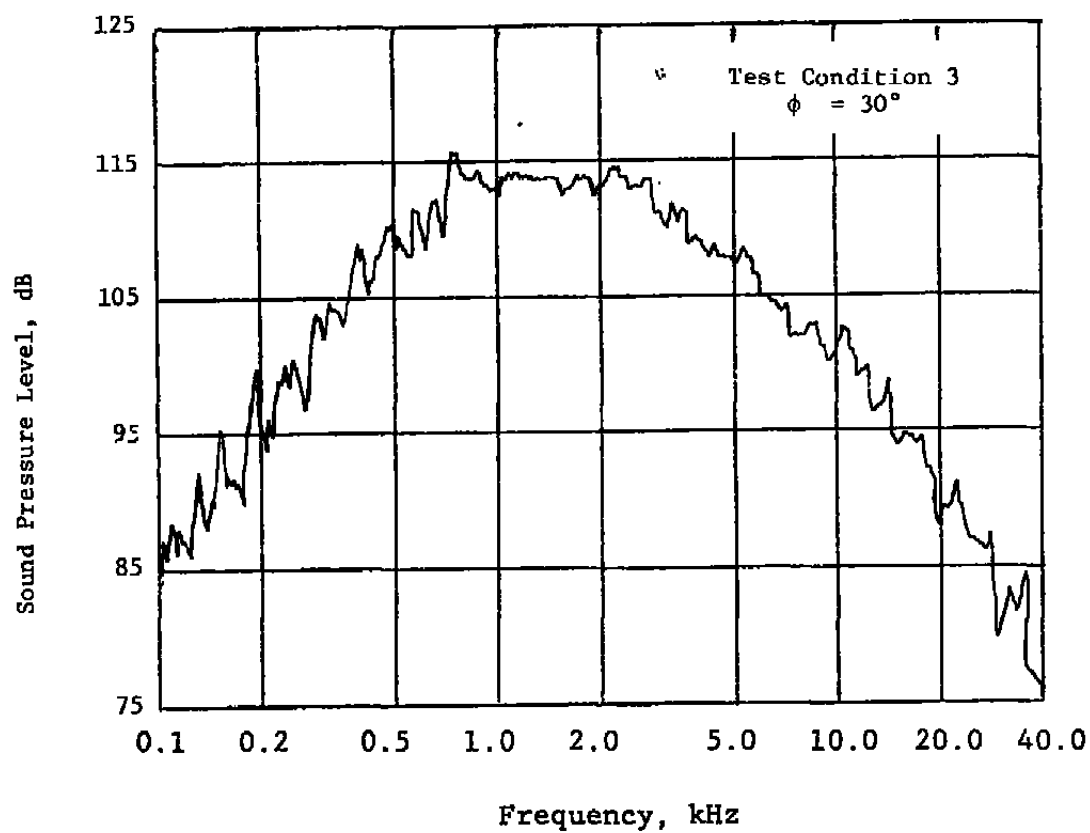
Fig. 4. Far Field Spectrum for Test Condition 3 at φ = 30°.

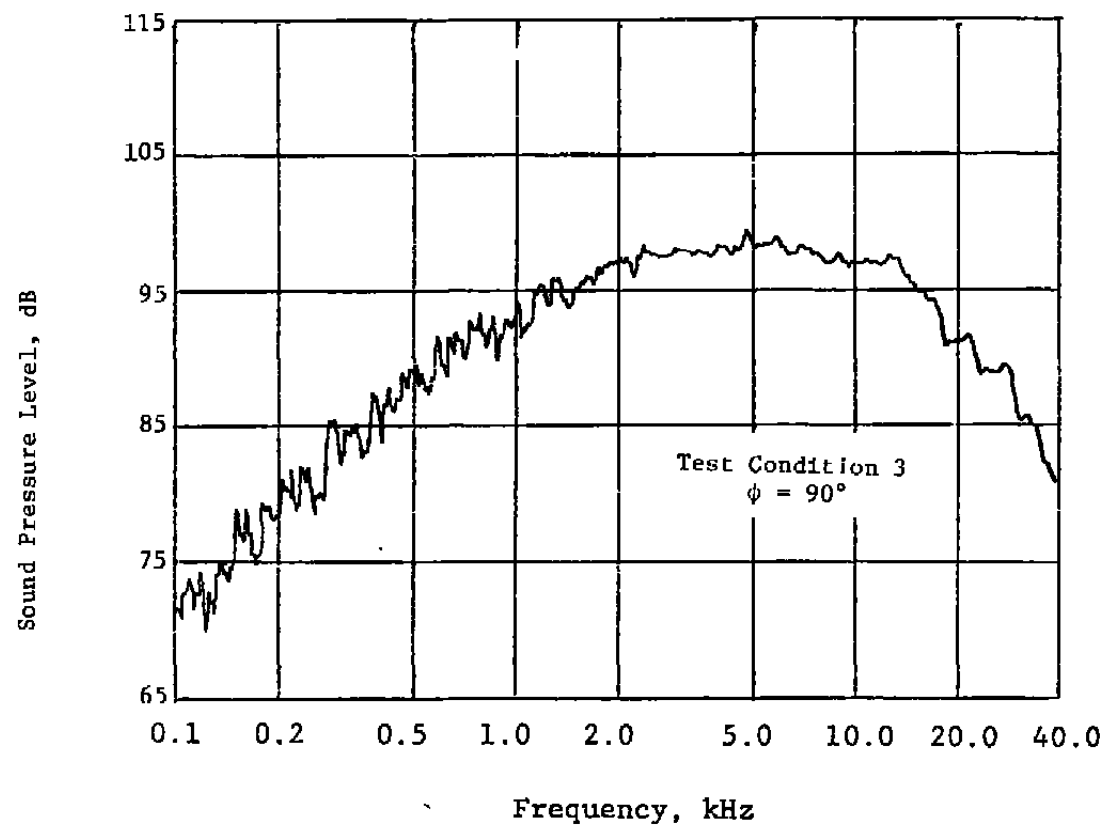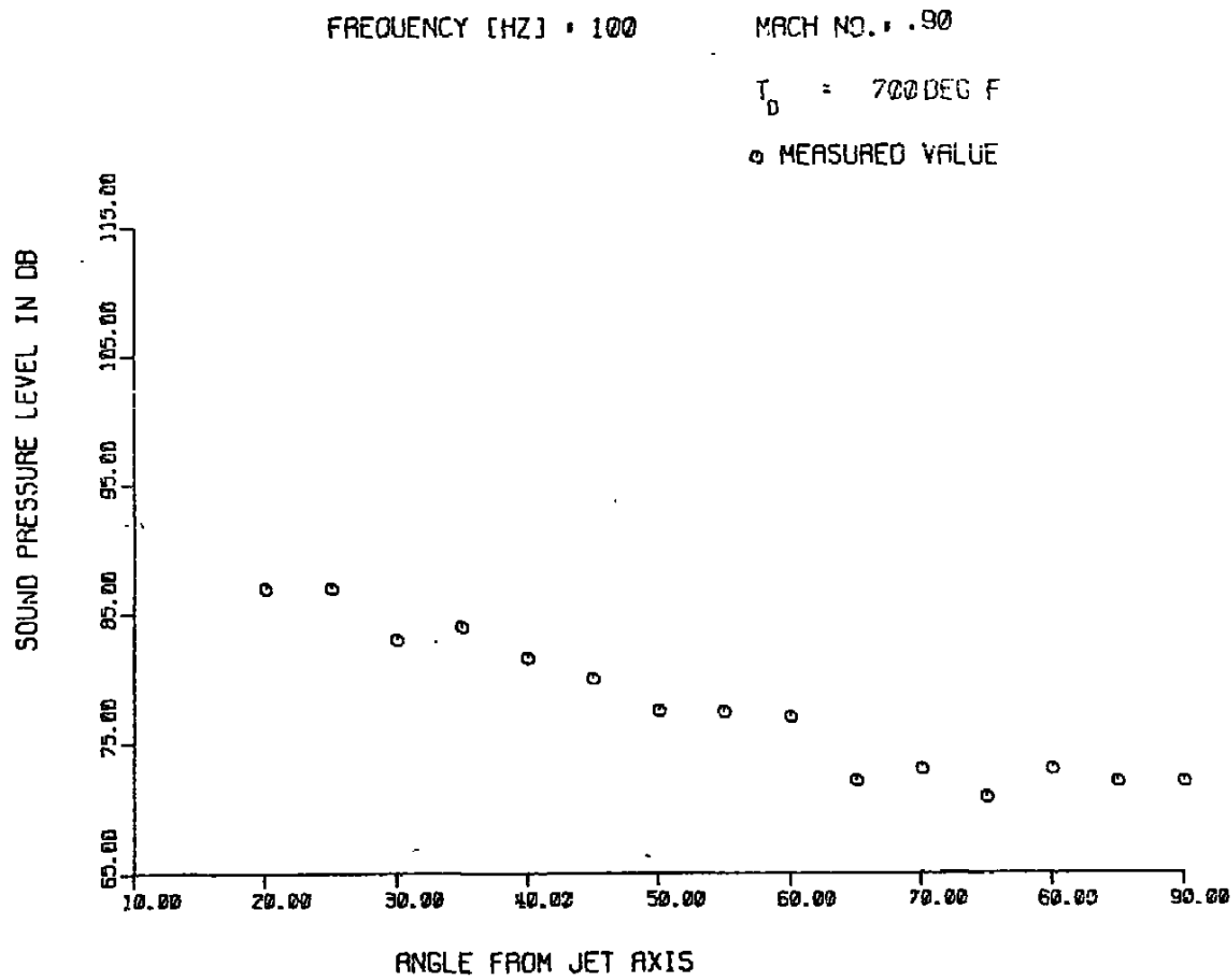Fig. 5. Far Field Spectrum for Test Condition 3 at $\phi = 60°$.

Fig. 6.   Far Field Spectrum for Test Condition 3 at $\phi = 90°$.

FREQUENCY [HZ] · 100   MACH NO. · .90

T_D =   700 DEG F

○ MEASURED VALUE

SOUND PRESSURE LEVEL IN DB

ANGLE FROM JET AXIS

Fig. 7.   One Third Octave Far Field Directivity for a Center Frequency of 100 Hz.   Test Condition 3.

FREQUENCY [HZ] : 1000   MACH NO. : .90

T_0 = 700 DEG F

⊙ MEASURED VALUE

SOUND PRESSURE LEVEL IN DB

ANGLE FROM JET AXIS
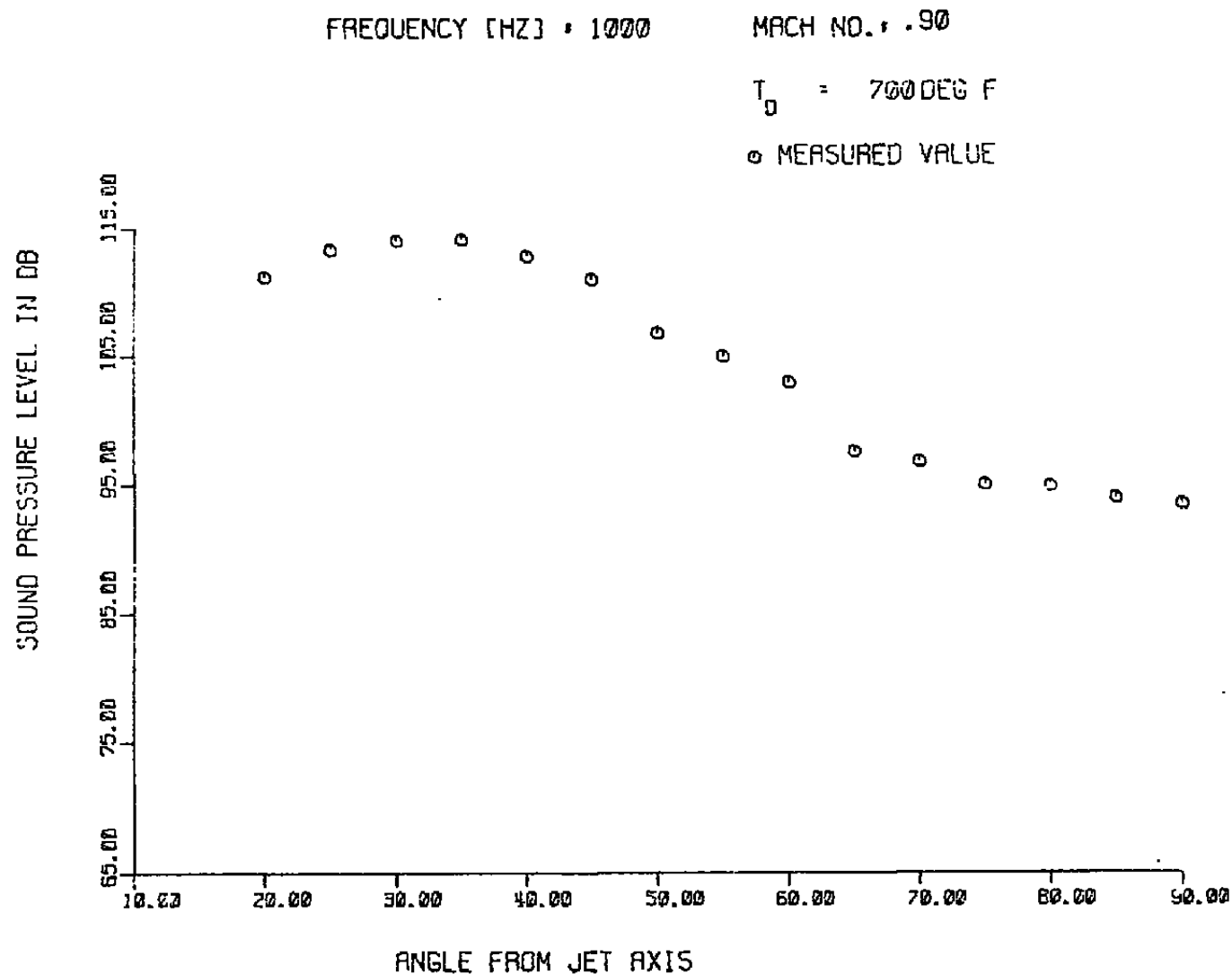
Fig. 8.   One Third Octave Far Field Directivity for a Center Frequency of 1000 Hz.   Test Condition 3.
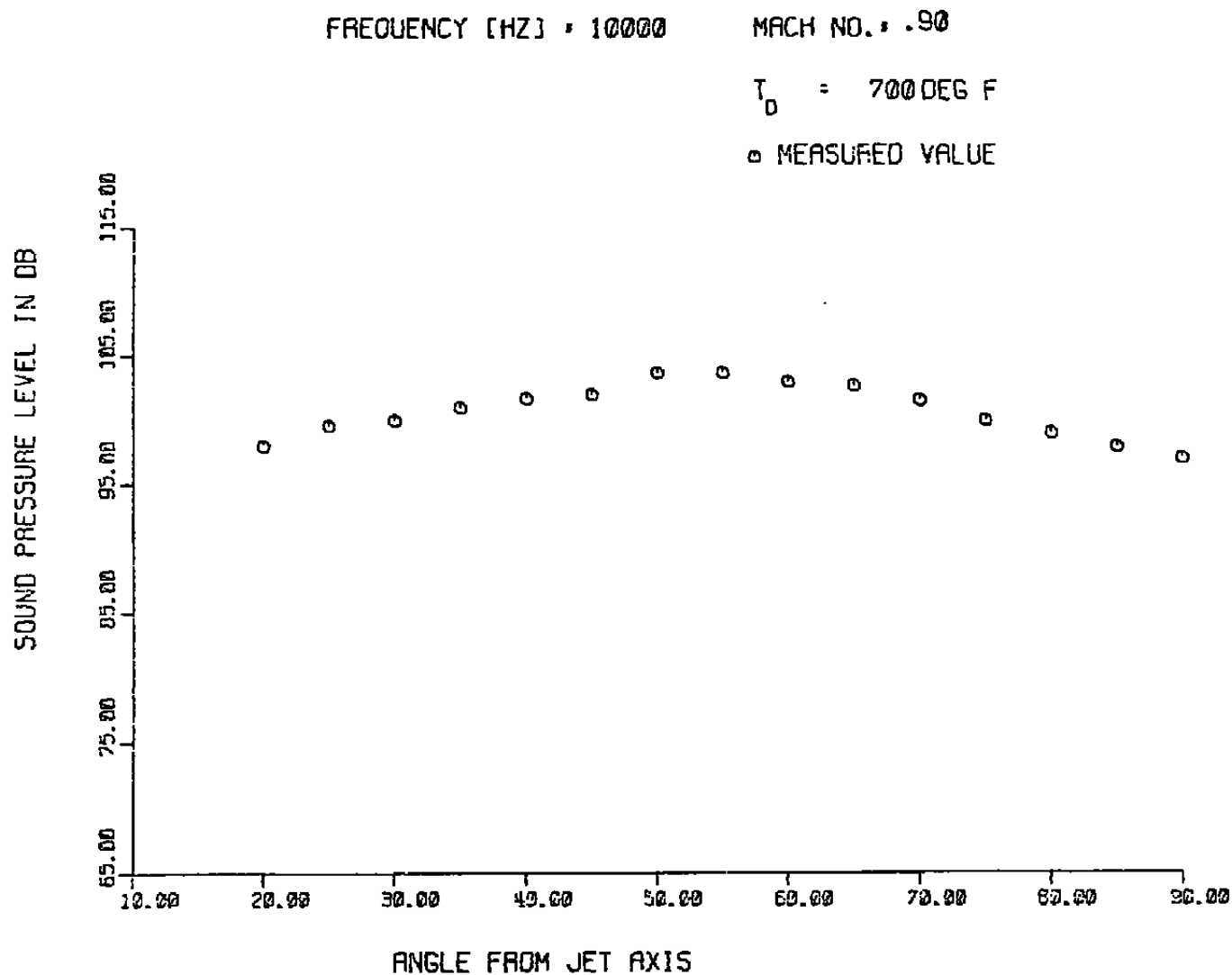
Fig. 9. One Third Octave Far Field Directivity for a Center Frequency of 10,000 Hz. Test Condition 3.
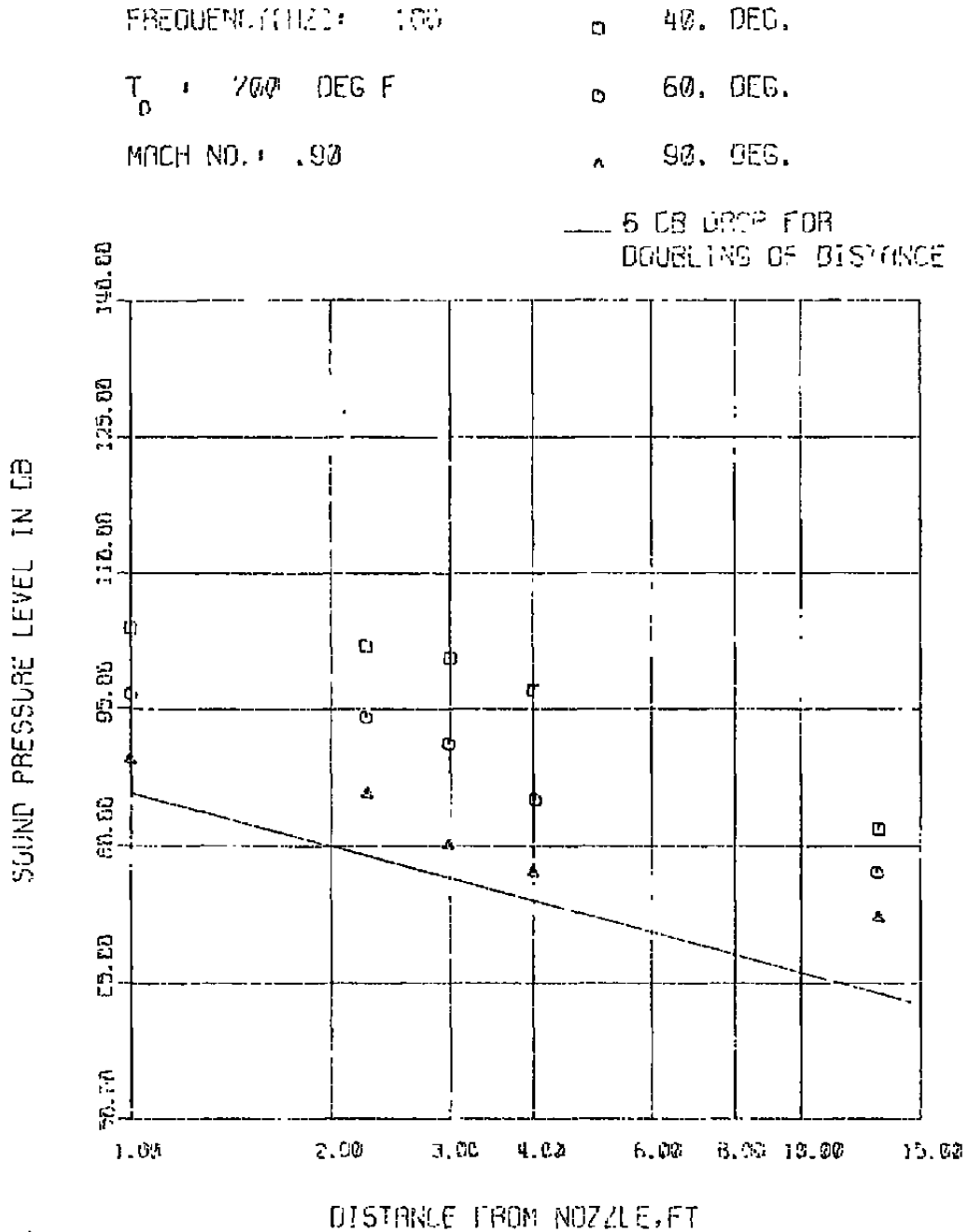
Fig. 10. Radial Variation of Sound Pressure Level for Test Condition 3 at 100 Hz.
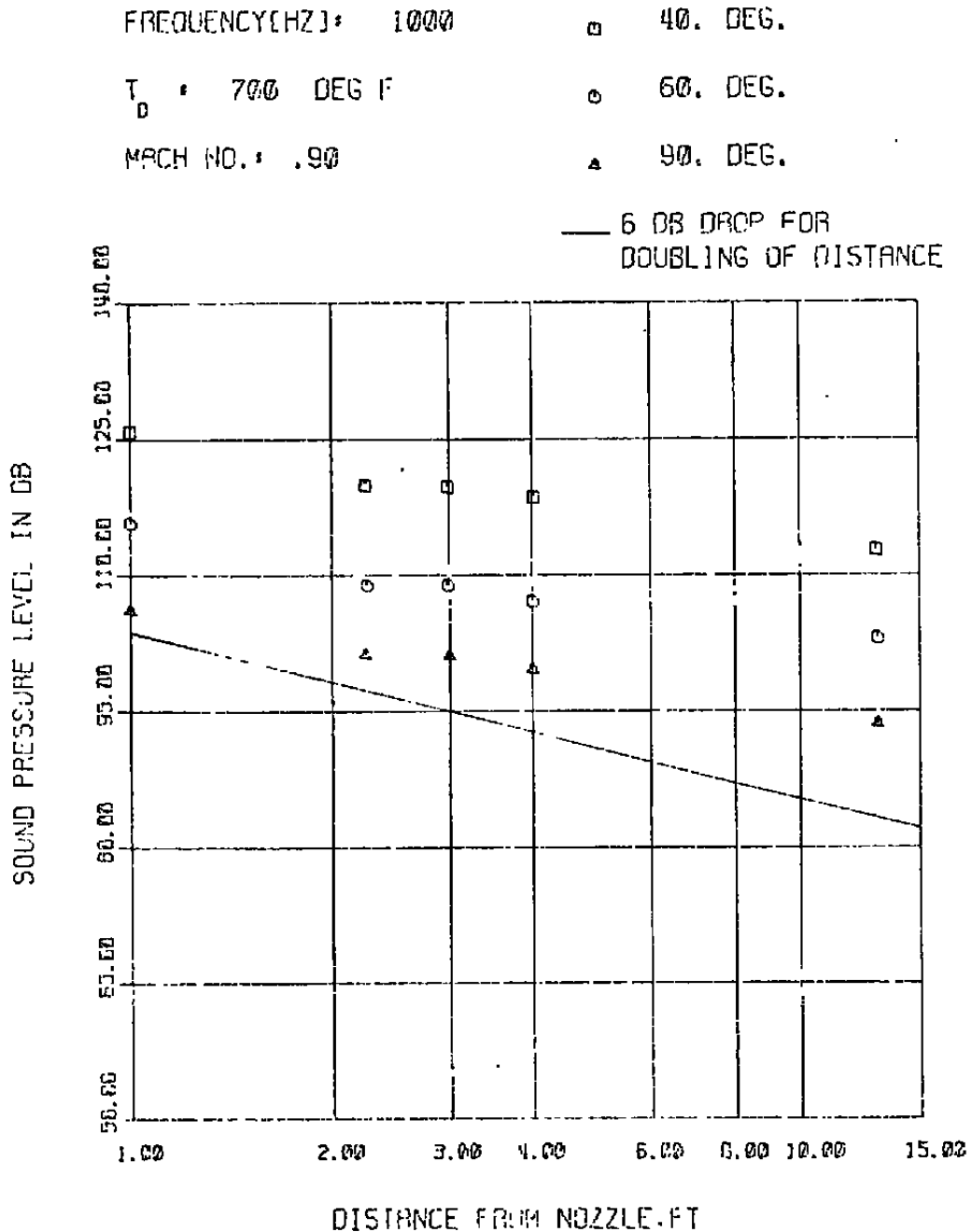
Fig. 11. Radial Variation of Sound Pressure Level for Test Condition 3 at 1000 Hz.
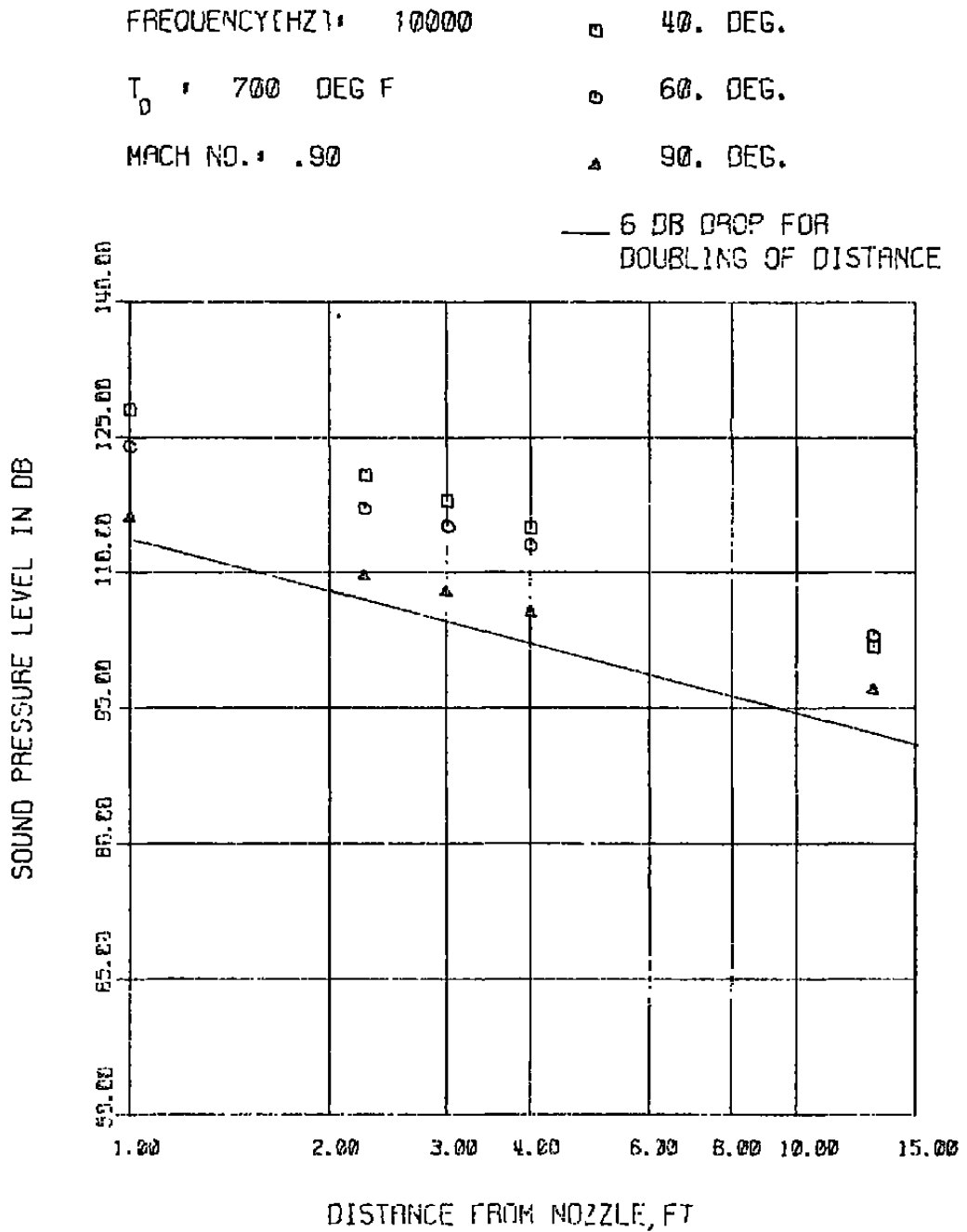
Fig. 12. Radial Variation of Sound Pressure Level for Test Condition 3 at 10,000 Hz.

FREQUENCY [HZ] = 100   MACH NO. = .90

T_0 = 70 DEG F

⊙ MEASURED VALUE

—— SYNTHESIZED DIRECTIVITY PATTERN

Nonzero Multipole Moments

$P_1 = 2.130 \times 10^3$

$Q_1 = 1.903 \times 10^3$

$A_2 = 4.088 \times 10^3$

$A_4 = 6.509 \times 10^4$
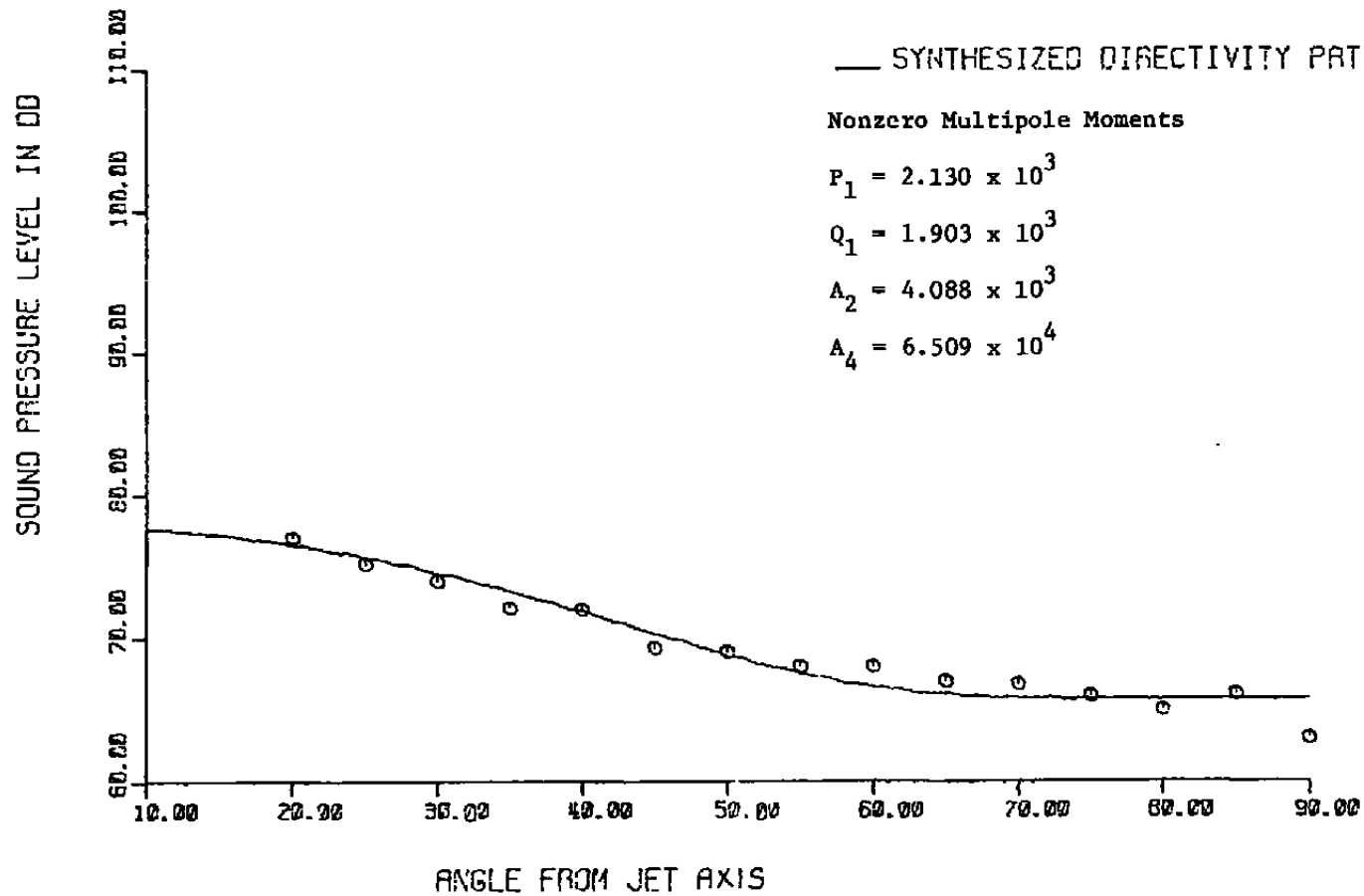
SOUND PRESSURE LEVEL IN DB

110.00
100.00
90.00
80.00
70.00
60.00

10.00   20.00   30.00   40.00   50.00   60.00   70.00   80.00   90.00

ANGLE FROM JET AXIS

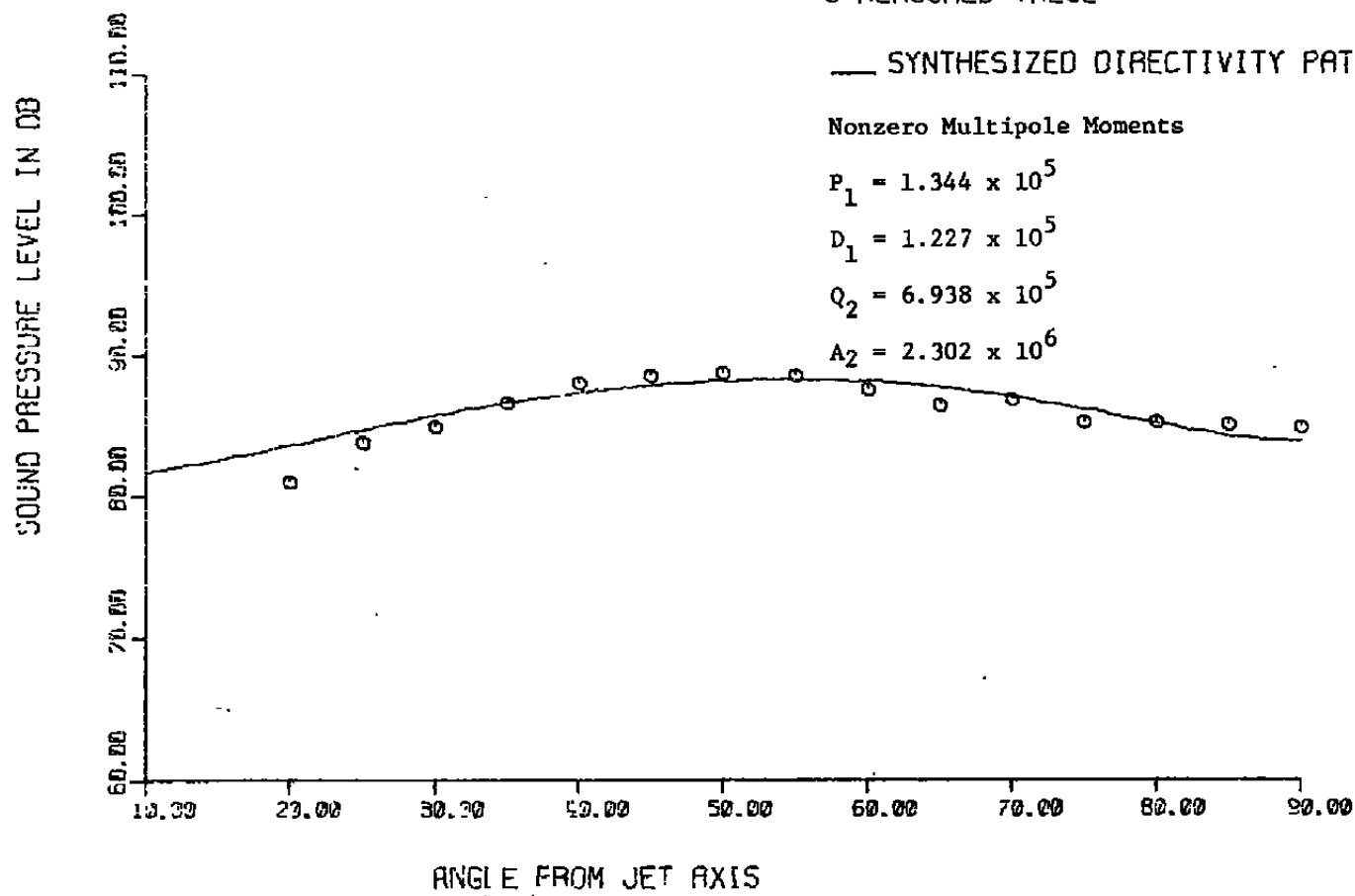Fig. 13.   Comparison of Measured Sound Pressure Level Directivity with Least Squares Fit for Test
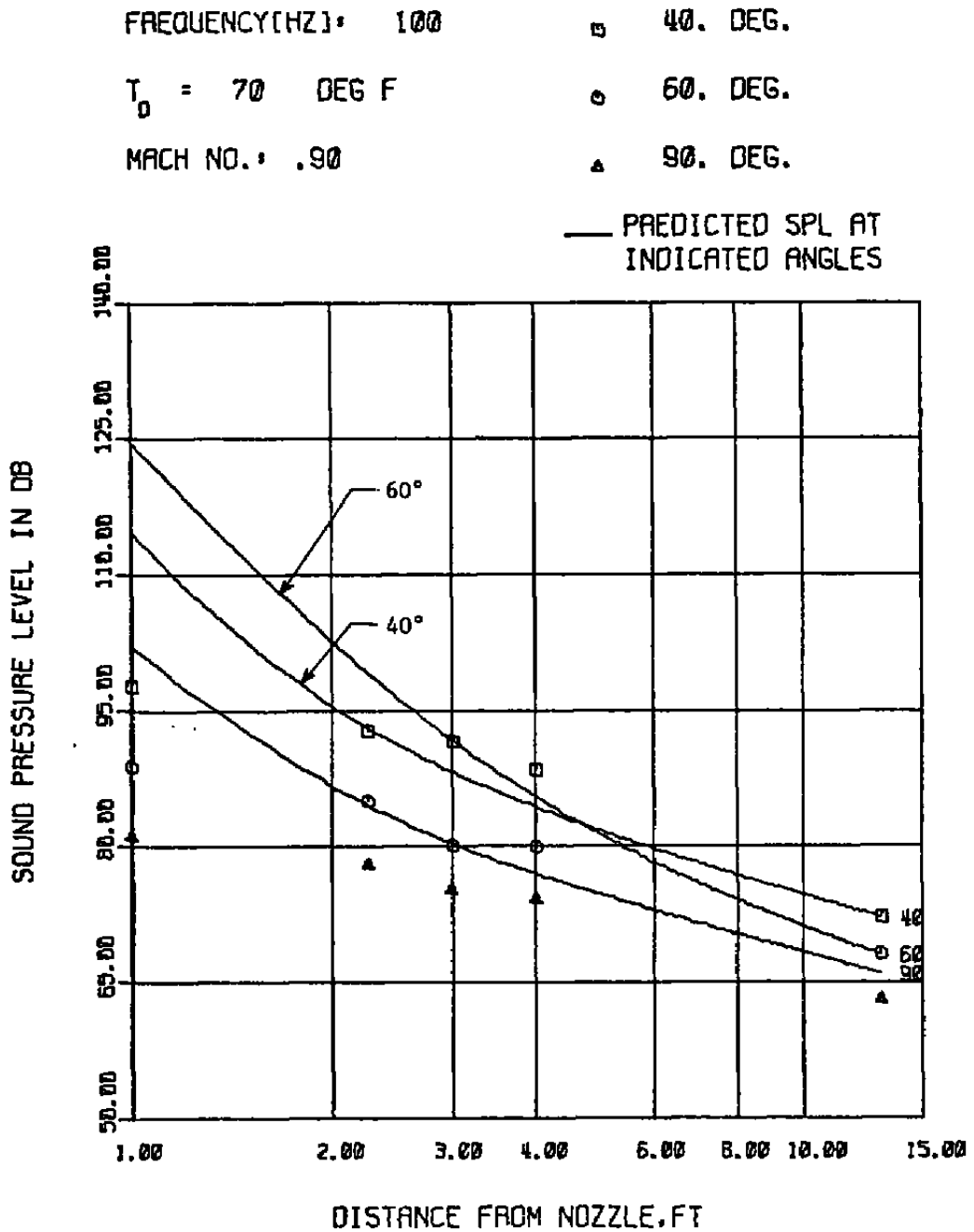Condition 2 at 100 Hz.

FREQUENCY [HZ] ⋅ 1000   MACH NO.: .90

T_D = 70 DEG F

⊙ MEASURED VALUE

___ SYNTHESIZED DIRECTIVITY PATTERN

Nonzero Multipole Moments

$P_1 = 2.681 \times 10^5$

$A_1 = 5.782 \times 10^4$

$A_4 = 1.332 \times 10^7$

SOUND PRESSURE LEVEL IN DB

ANGLE FROM JET AXIS

44
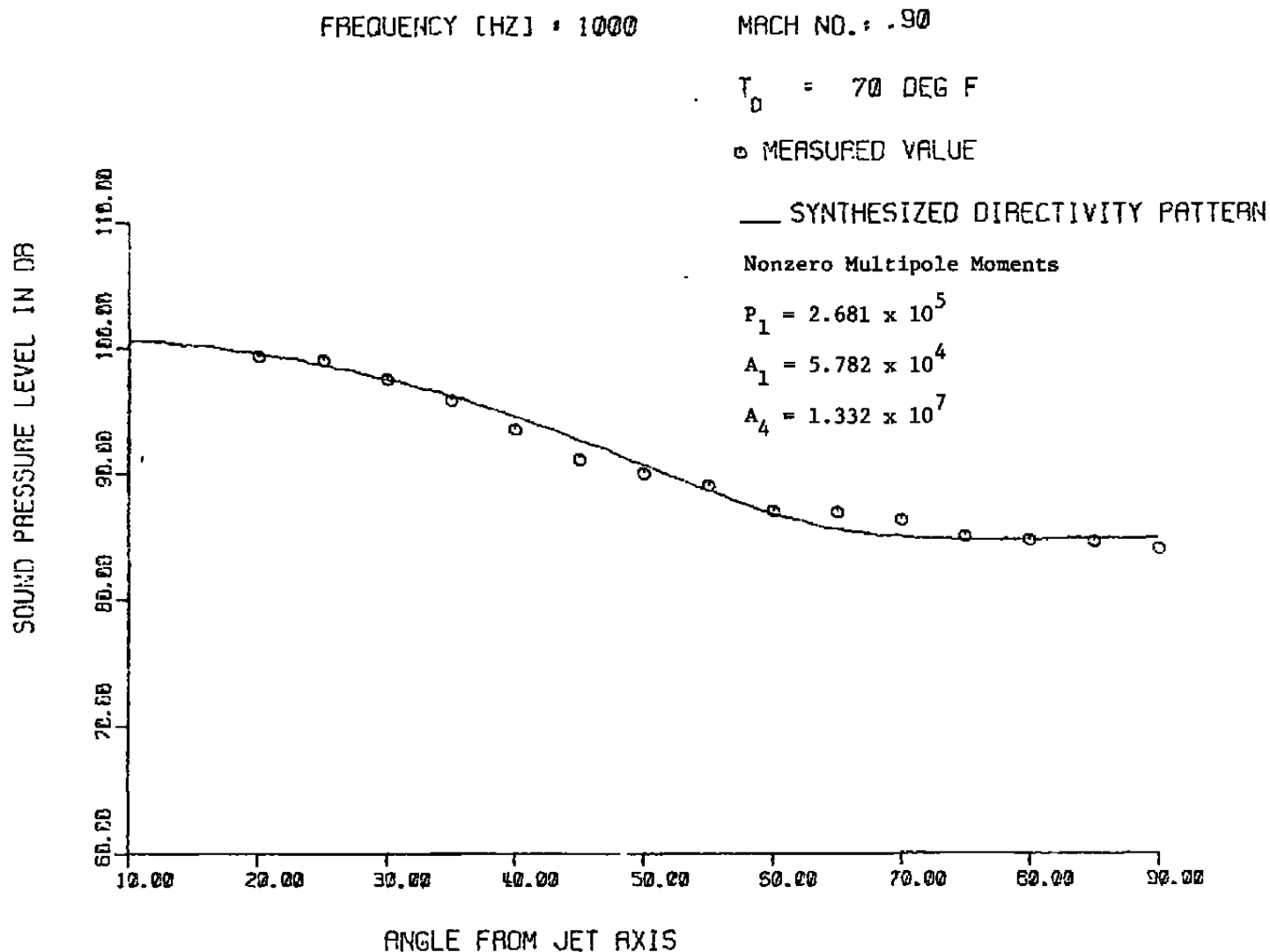
Fig. 14. Comparison of Measured Sound Pressure Level Directivity with Least Squares Fit for Test
Condition 2 at 1000 Hz.

FREQUENCY [HZ] : 10000   MACH NO. : .90

T_0 = 70 DEG F

⊙ MEASURED VALUE

___ SYNTHESIZED DIRECTIVITY PATTERN

Nonzero Multipole Moments

$P_1 = 1.344 \times 10^5$

$D_1 = 1.227 \times 10^5$

$Q_2 = 6.938 \times 10^5$

$A_2 = 2.302 \times 10^6$

Fig. 15. Comparison of Measured Sound Pressure Level Directivity with Least Squares Fit for Test Condition 2 at 10,000 Hz.

Fig. 16. Comparison of Measured and Predicted Sound Pressure Levels for
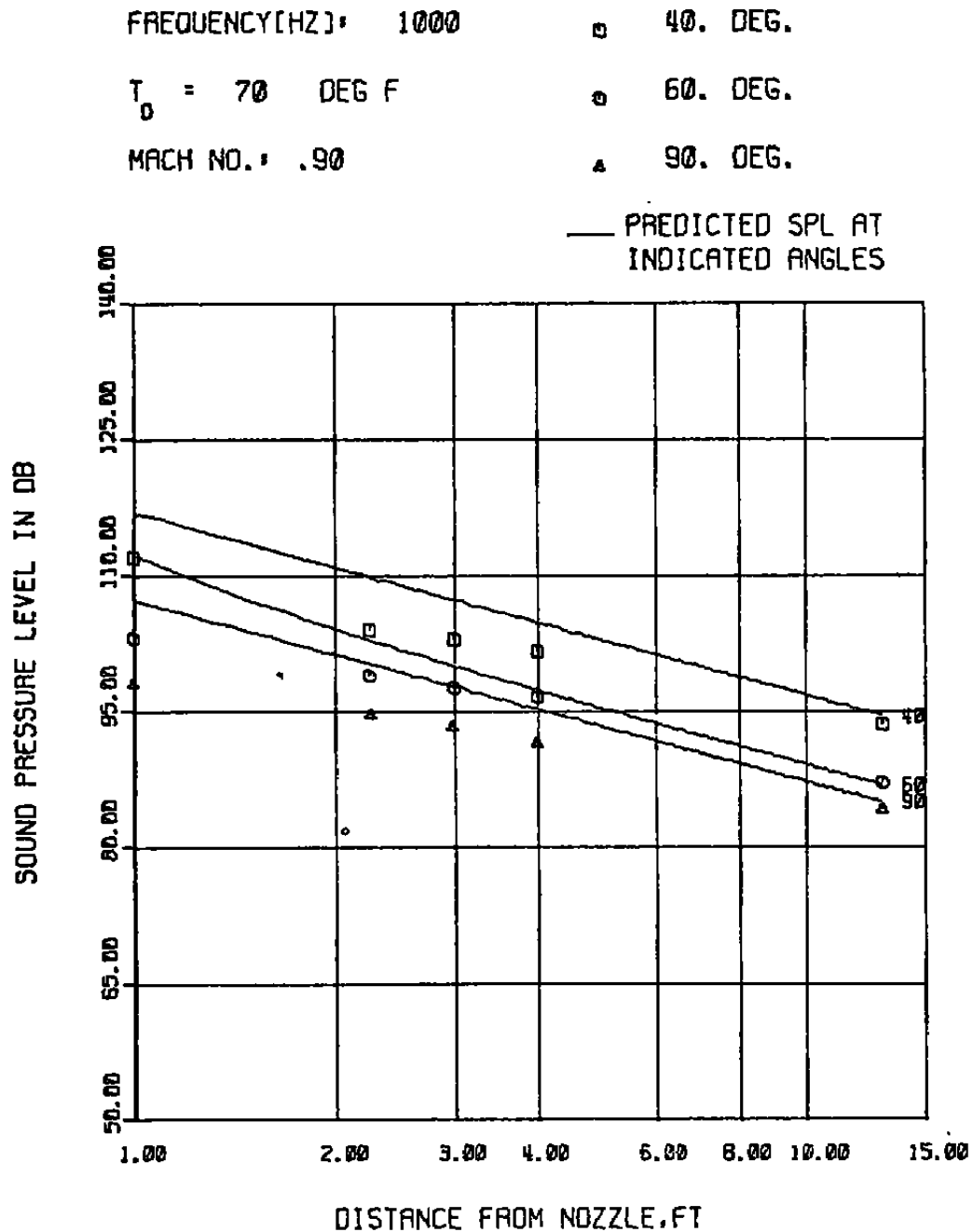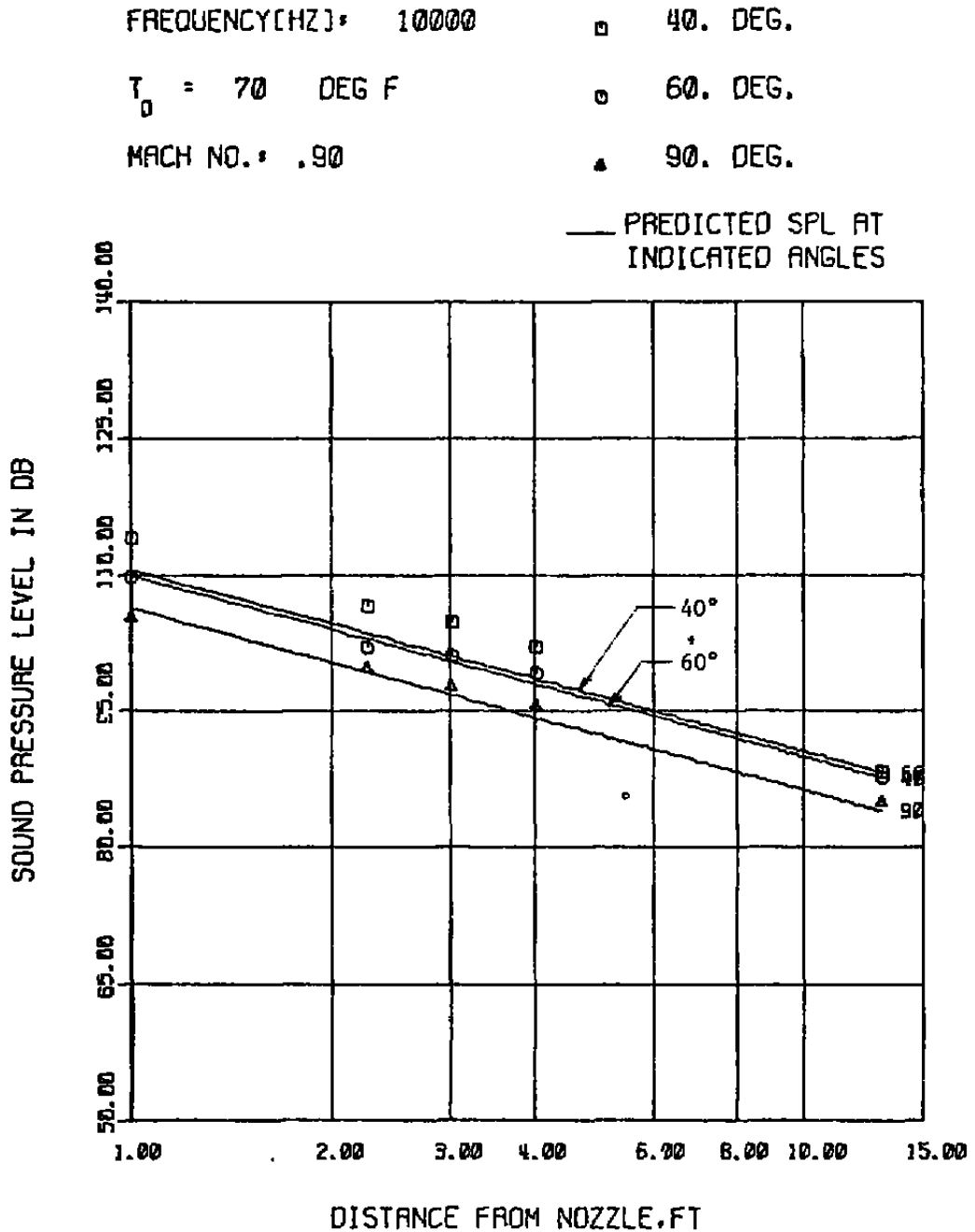Test Condition 2 at 100 Hz.

Fig. 17. Comparison of Measured and Predicted Sound Pressure Levels for Test Condition 2 at 1000 Hz.

Fig. 18.   Comparison of Measured and Predicted Sound Pressure Levels
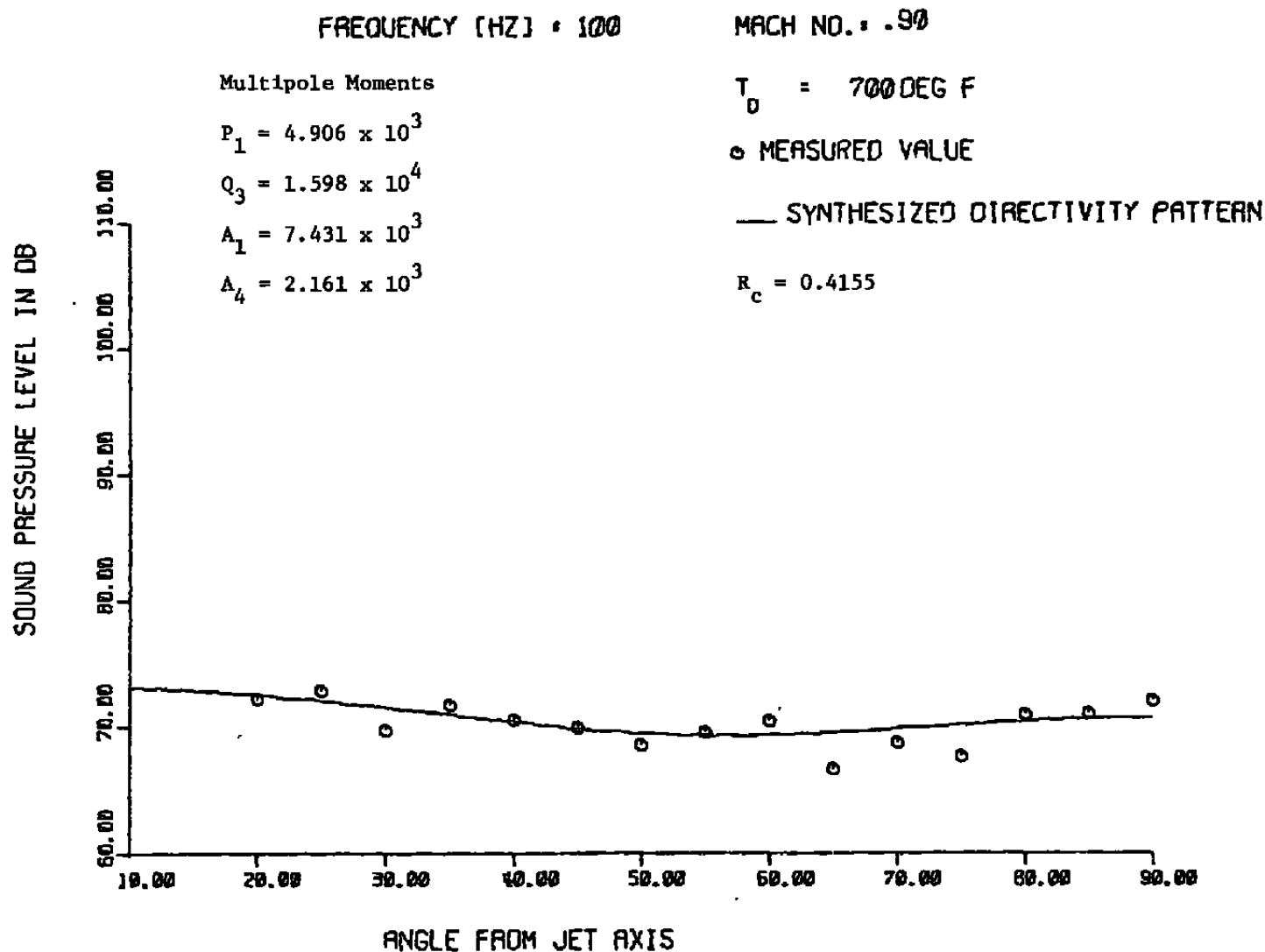for Test Condition 2 at 10,000 Hz.

Fig. 19. Comparison of Measured Far Field Sound Directivity after Removal of Convection Effects with Least Squares Fit for Test Condition 3 at 100 Hz.
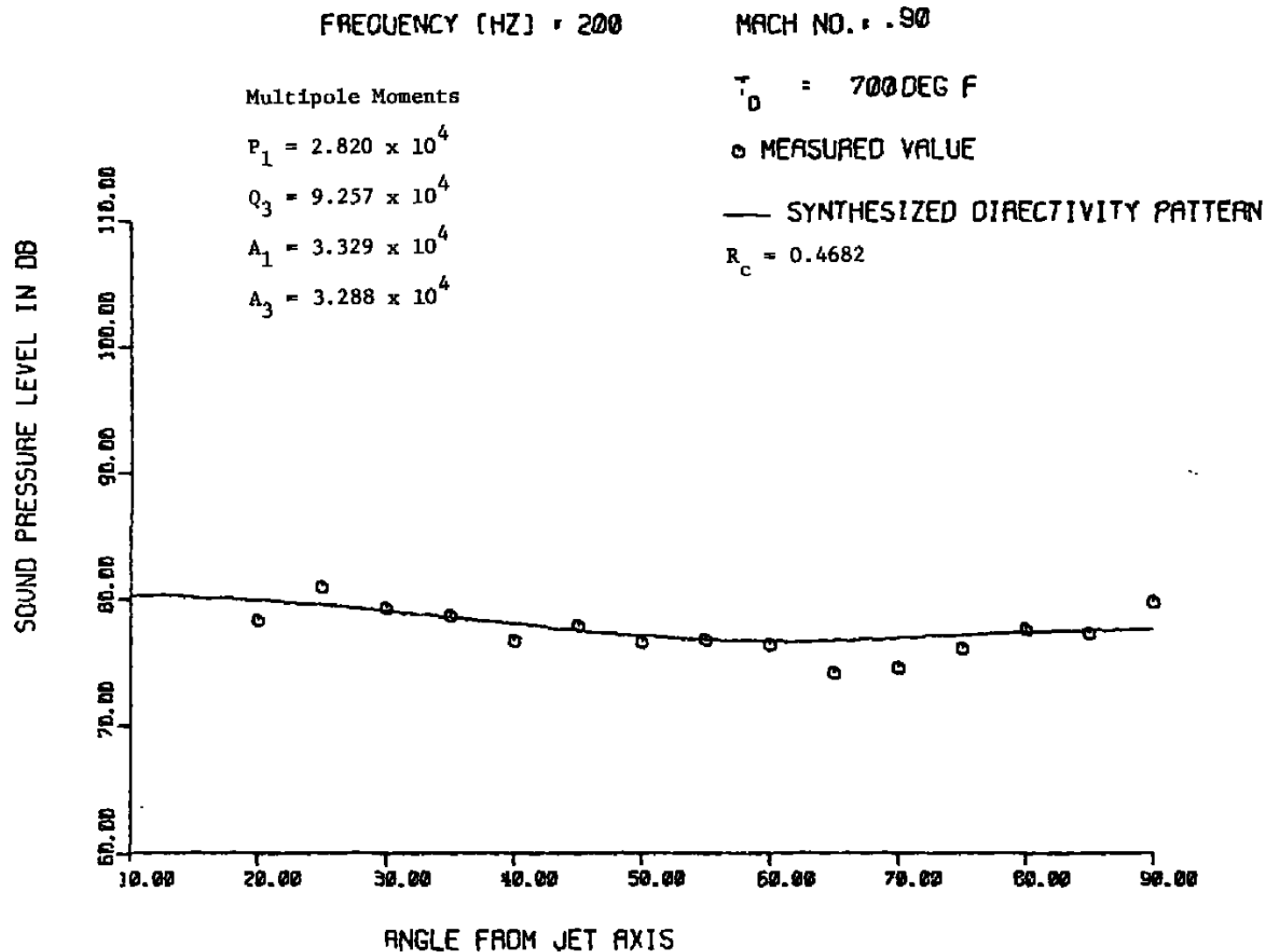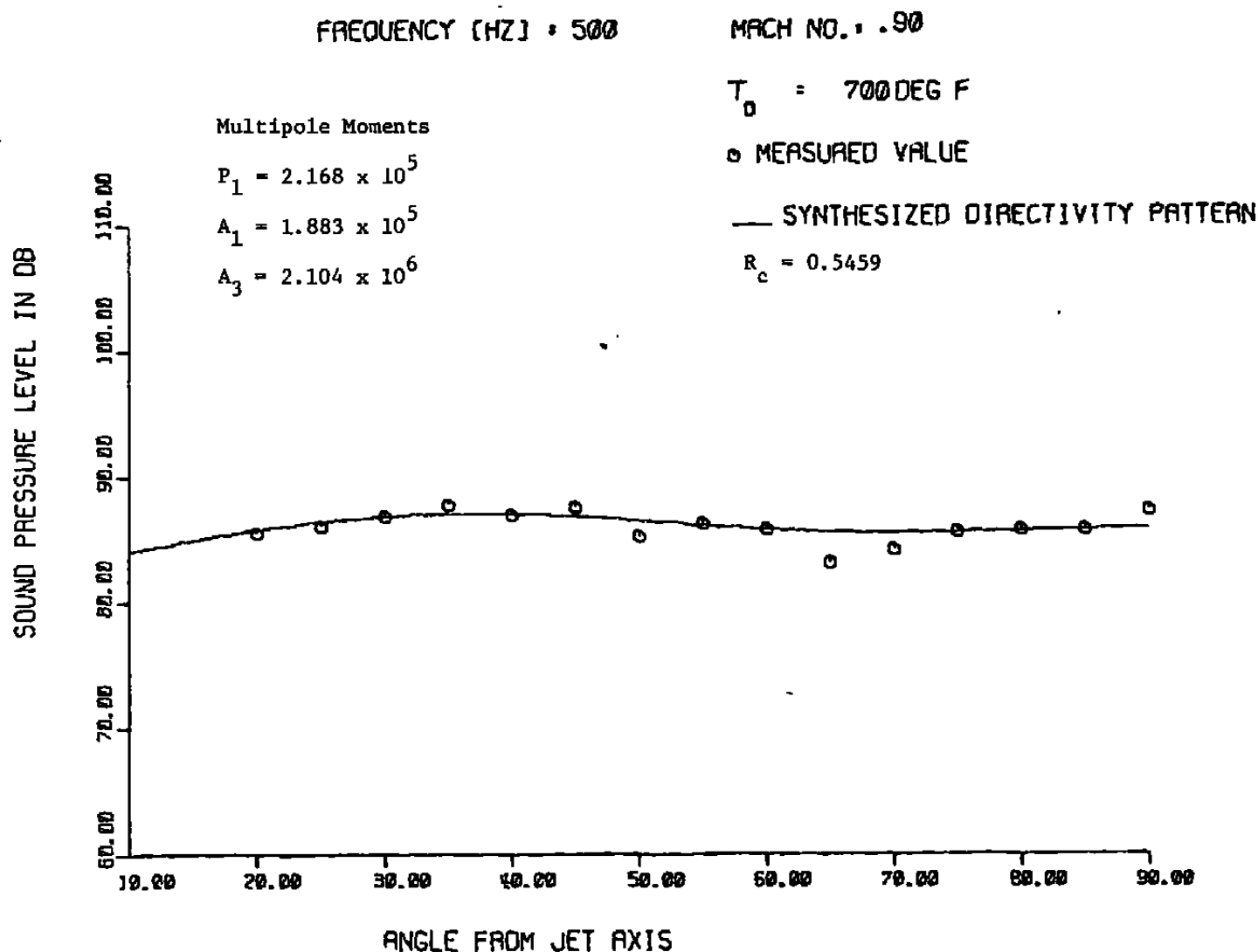
FREQUENCY [HZ] · 200   MACH NO. · .90

Multipole Moments

T_D = 700 DEG F

P_1 = 2.820 x 10^4

⊙ MEASURED VALUE

Q_3 = 9.257 x 10^4

—— SYNTHESIZED DIRECTIVITY PATTERN

A_1 = 3.329 x 10^4

R_c = 0.4682

A_3 = 3.288 x 10^4

SOUND PRESSURE LEVEL IN DB

110.00
100.00
90.00
80.00
70.00
60.00

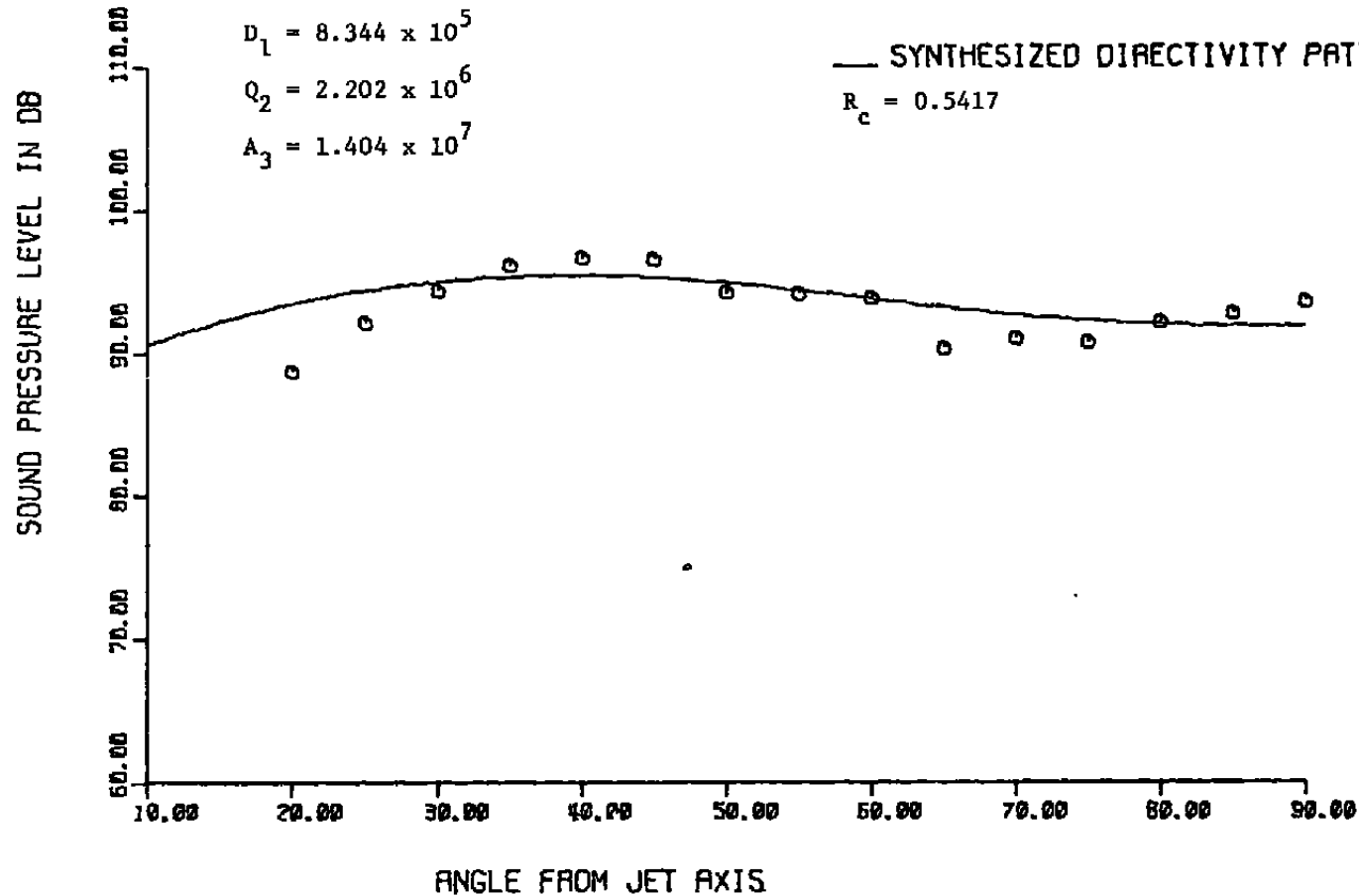10.00   20.00   30.00   40.00   50.00   60.00   70.00   80.00   90.00

ANGLE FROM JET AXIS

Fig. 20.   Comparison of Measured Far Field Sound Directivity after Removal of Convection Effects with Least Squares Fit for Test Condition 3 at 200 Hz.

FREQUENCY [HZ] ≥ 500   MACH NO. ≥ .90

T_0 = 700 DEG F

Multipole Moments

○ MEASURED VALUE

P_1 = 2.168 x 10^5

___ SYNTHESIZED DIRECTIVITY PATTERN

A_1 = 1.883 x 10^5

R_c = 0.5459

A_3 = 2.104 x 10^6

SOUND PRESSURE LEVEL IN DB

ANGLE FROM JET AXIS

Fig. 21. Comparison of Measured Far Field Sound Directivity after Removal of Convection Effects with Least Squares Fit for Test Condition 3 at 500 Hz.

FREQUENCY (HZ) · 1000   MACH NO. · .90

Multipole Moments

P_1 = 7.815 x 10^5

D_1 = 8.344 x 10^5

Q_2 = 2.202 x 10^6

A_3 = 1.404 x 10^7

T_0 = 700 DEG F

⊙ MEASURED VALUE

—— SYNTHESIZED DIRECTIVITY PATTERN

R_c = 0.5417

Fig. 22. Comparison of Measured Far Field Sound Directivity after Removal of Convection Effects with
Least Squares Fit for Test Condition 3 at 1000 Hz.

Test Condition 3

f = 100 Hz
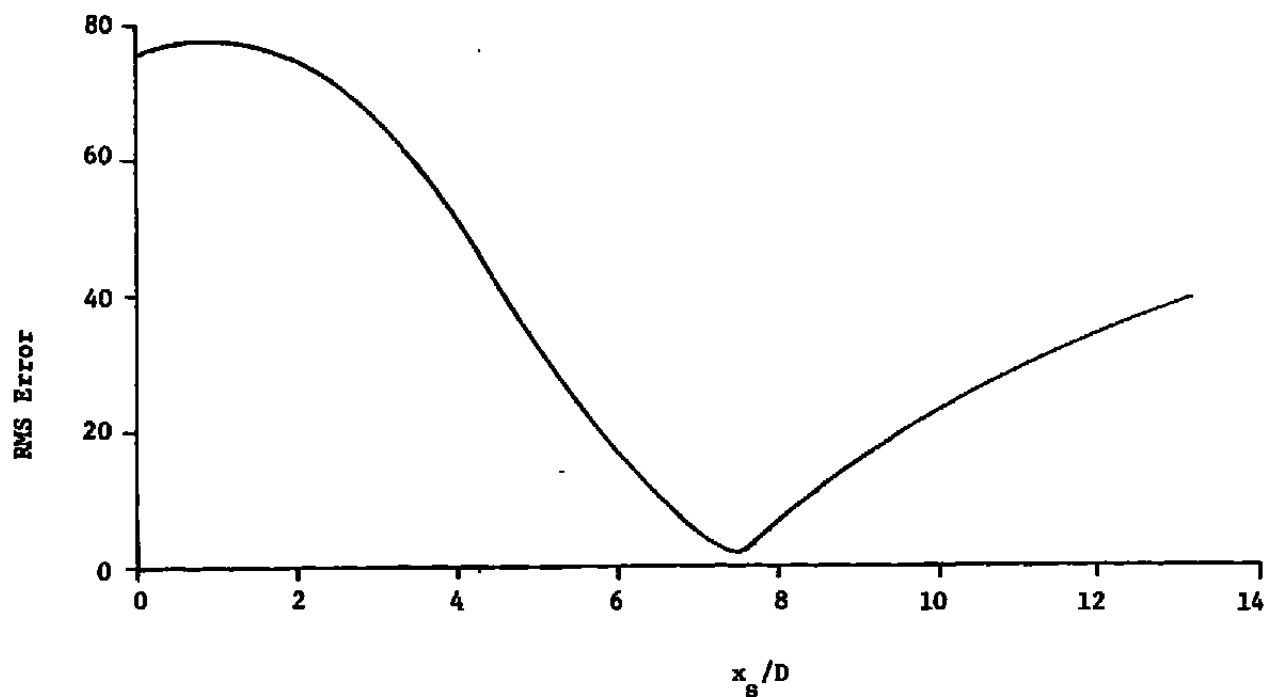
Fig. 23. RMS Error Between Microphone Data at 1 foot and Predicted Sound Level as a Function of Assumed Source Location for 100 Hz.

Test Condition		Mach No.	Stagnation Temp (°F)
□	4	0.95	800.0
△	1	0.70	80.0
○	3	0.90	700.0
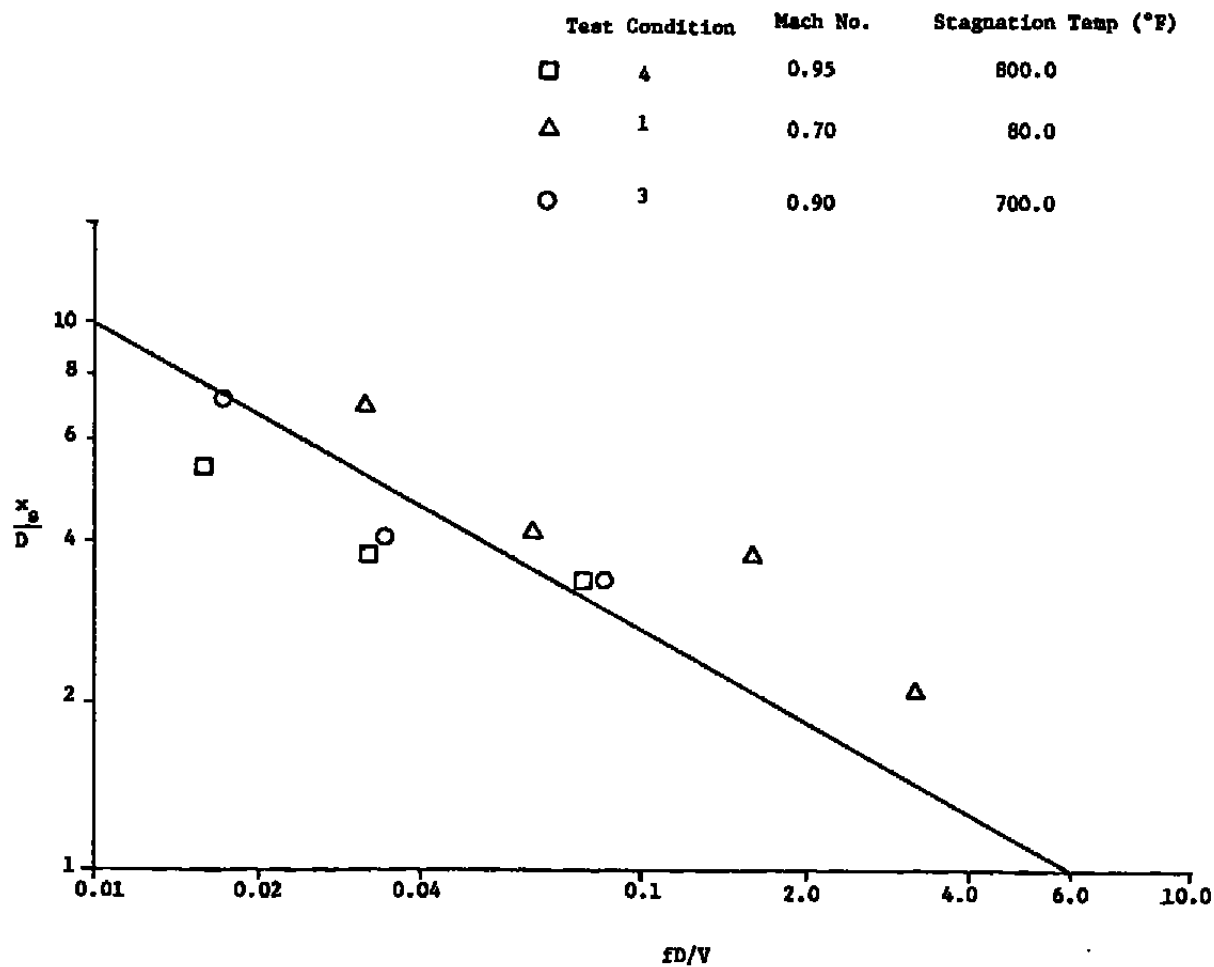
Fig. 24. Optimum Source Location as a Function of Strouhal Number.

FREQUENCY[HZ]: 100   □   40. DEG.

T_0 = 80   DEG F   ○   60. DEG.

MACH NO.: .70   ▲   90. DEG.
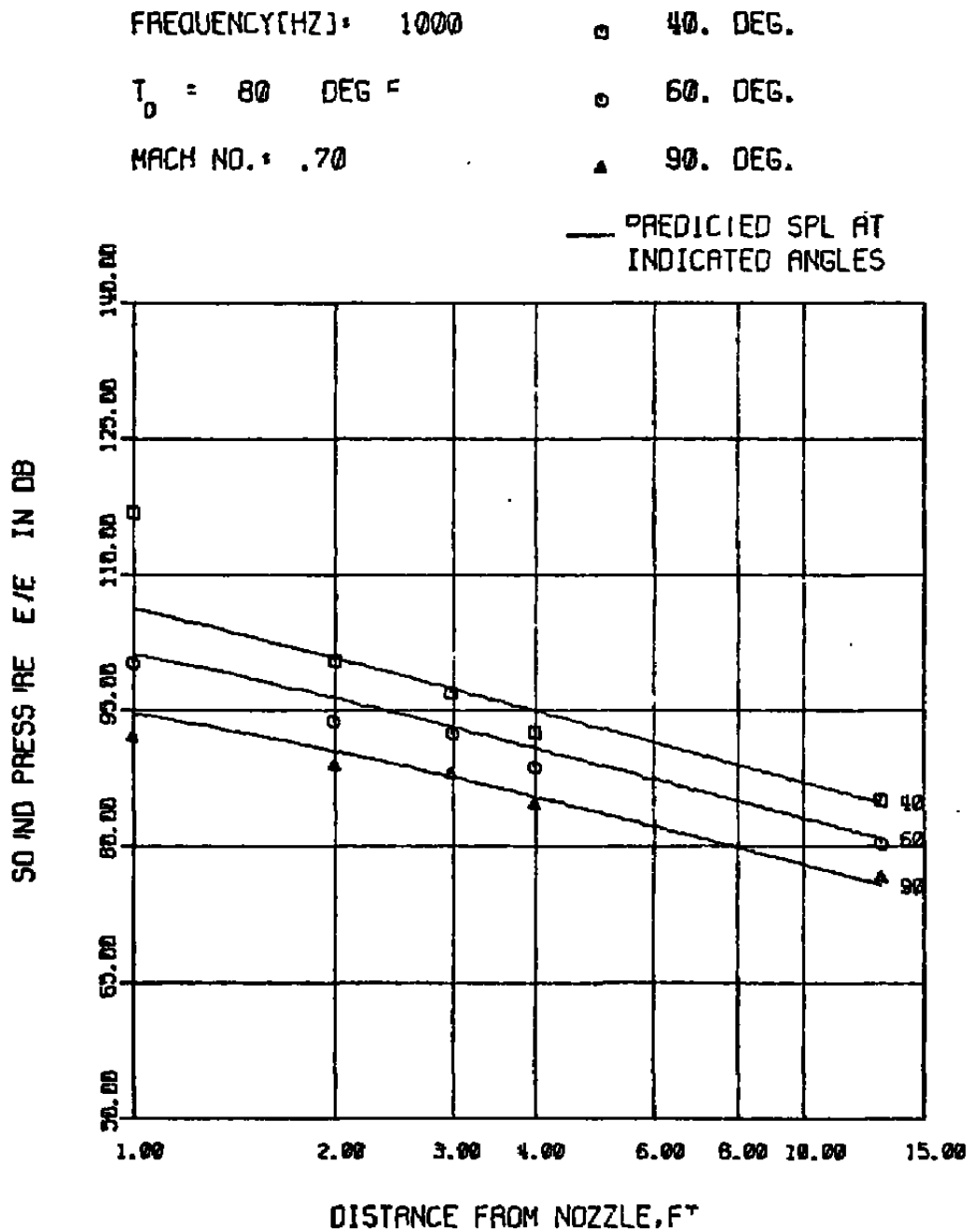
———— PREDICTED SPL AT
      INDICATED ANGLES
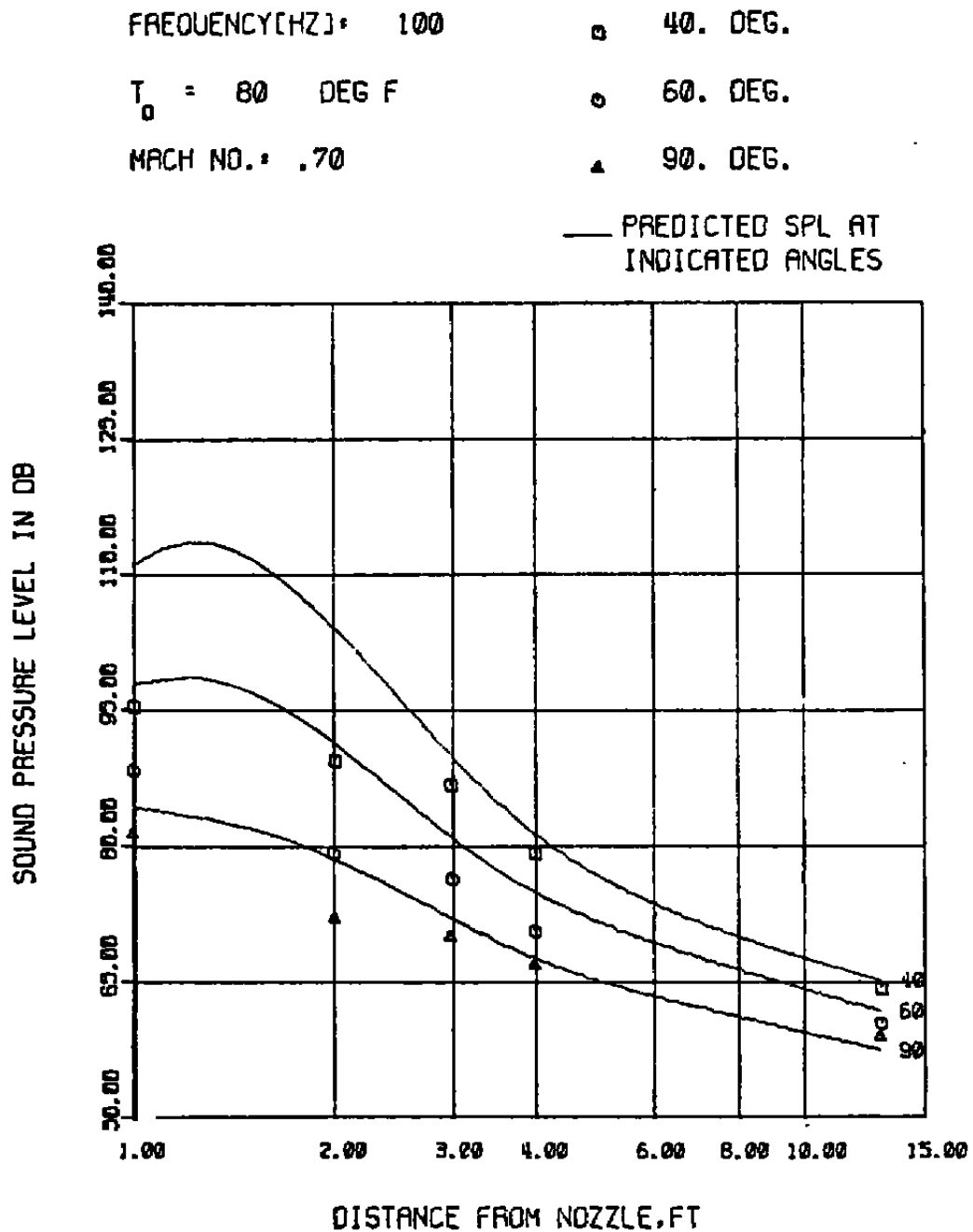
Fig. 25.   Comparison of Measured and Predicted Sound Pressure Levels using
           Modified Source Modeling Technique for Test Condition 1 at 100 Hz.
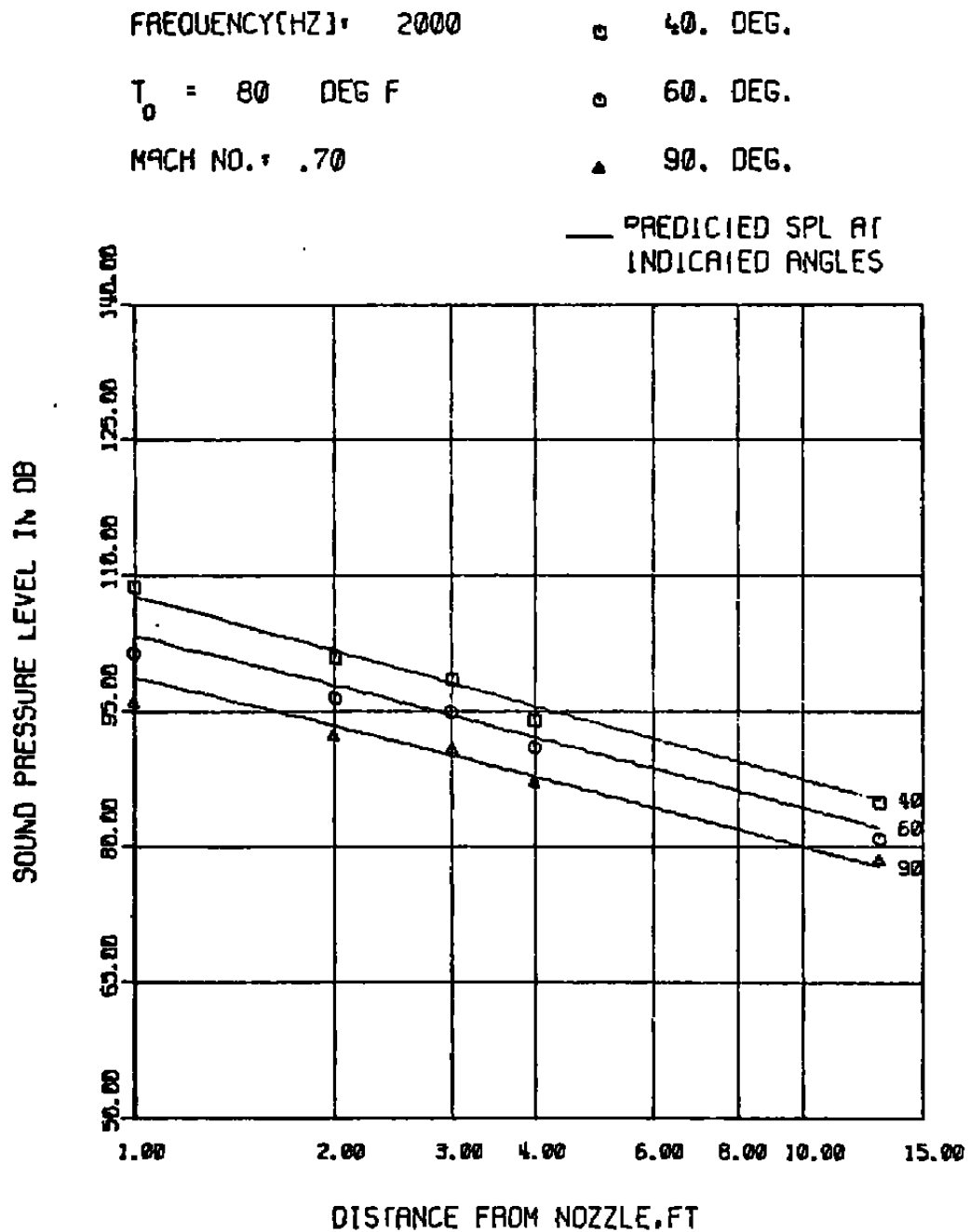
FREQUENCY(HZ): 200   □   40. DEG.

T_0 = 80   DEG F   ○   60. DEG.

MACH NO. = .70   ▲   90. DEG.

—— PREDICTED SPL AT
INDICATED ANGLES
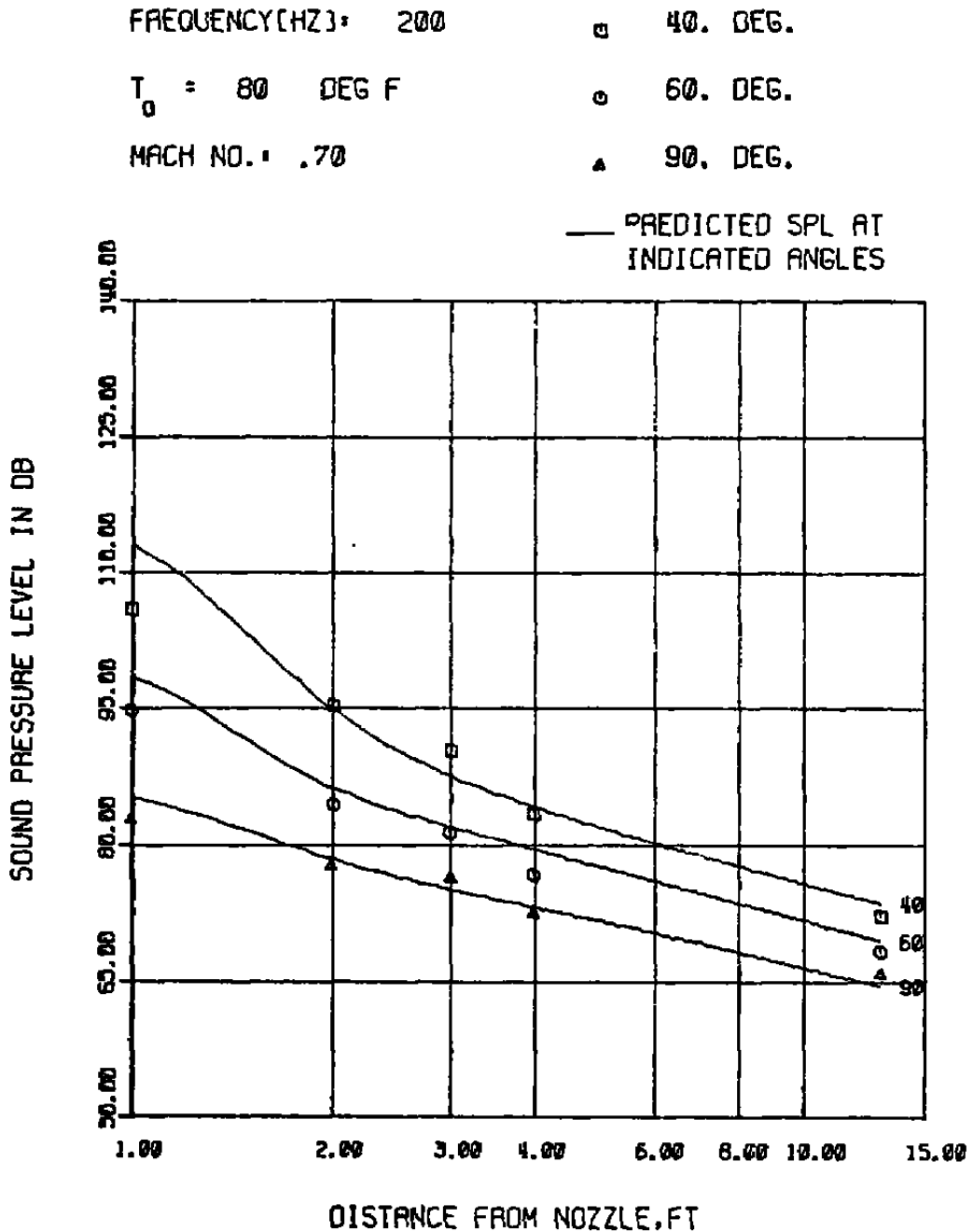
Fig. 26. Comparison of Measured and Predicted Sound Pressure Levels using Modified Source Modeling Technique for Test Condition 1 at 200 Hz.
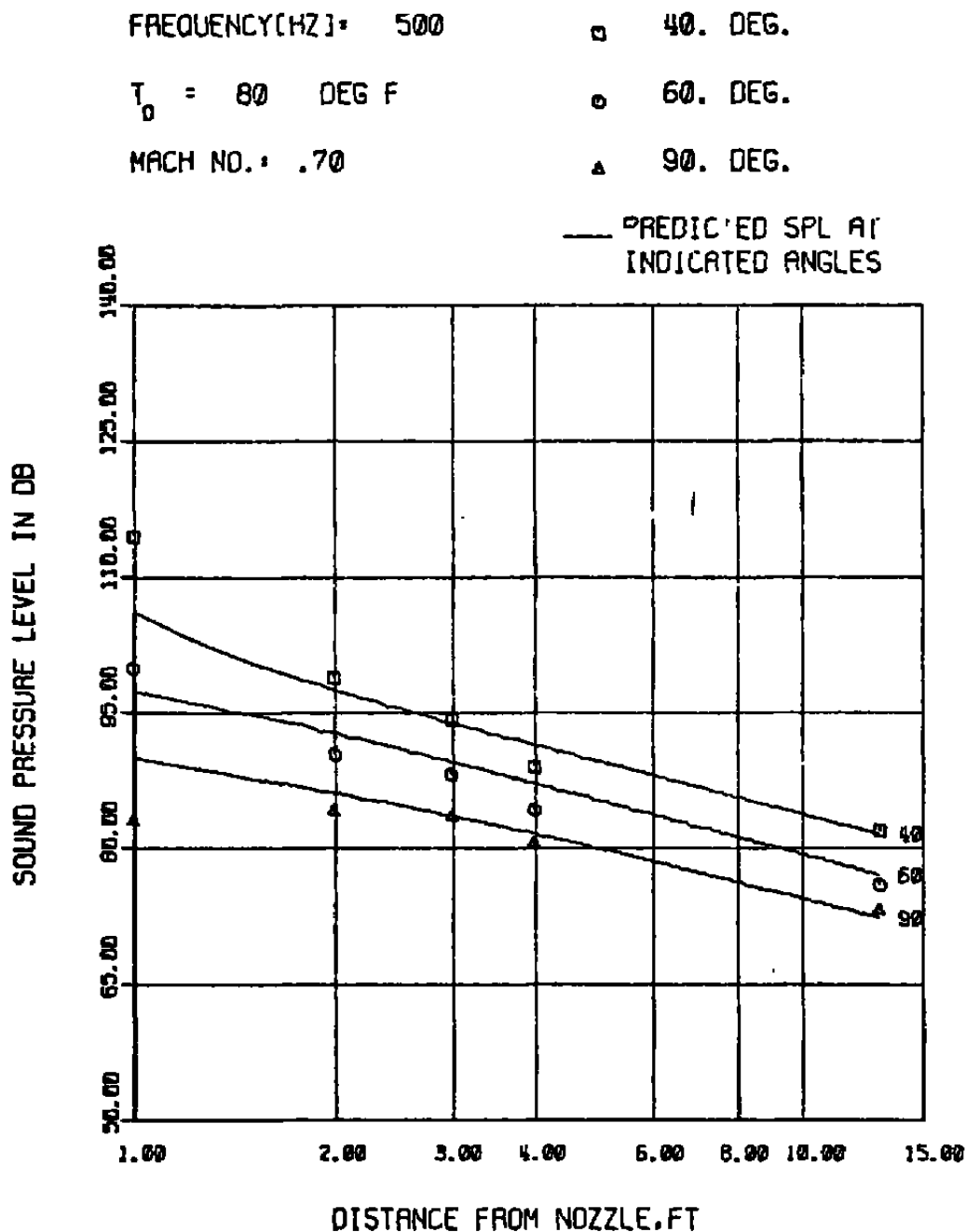
Fig. 27. Comparison of Measured and Predicted Sound Pressure Levels using Modified Source Modeling Technique for Test Condition 1 at 500 Hz.

FREQUENCY(HZ): 1000   ◻   40. DEG.

T$_D$ = 80 DEG F   ◦   60. DEG.

MACH NO.: .70   ▲   90. DEG.
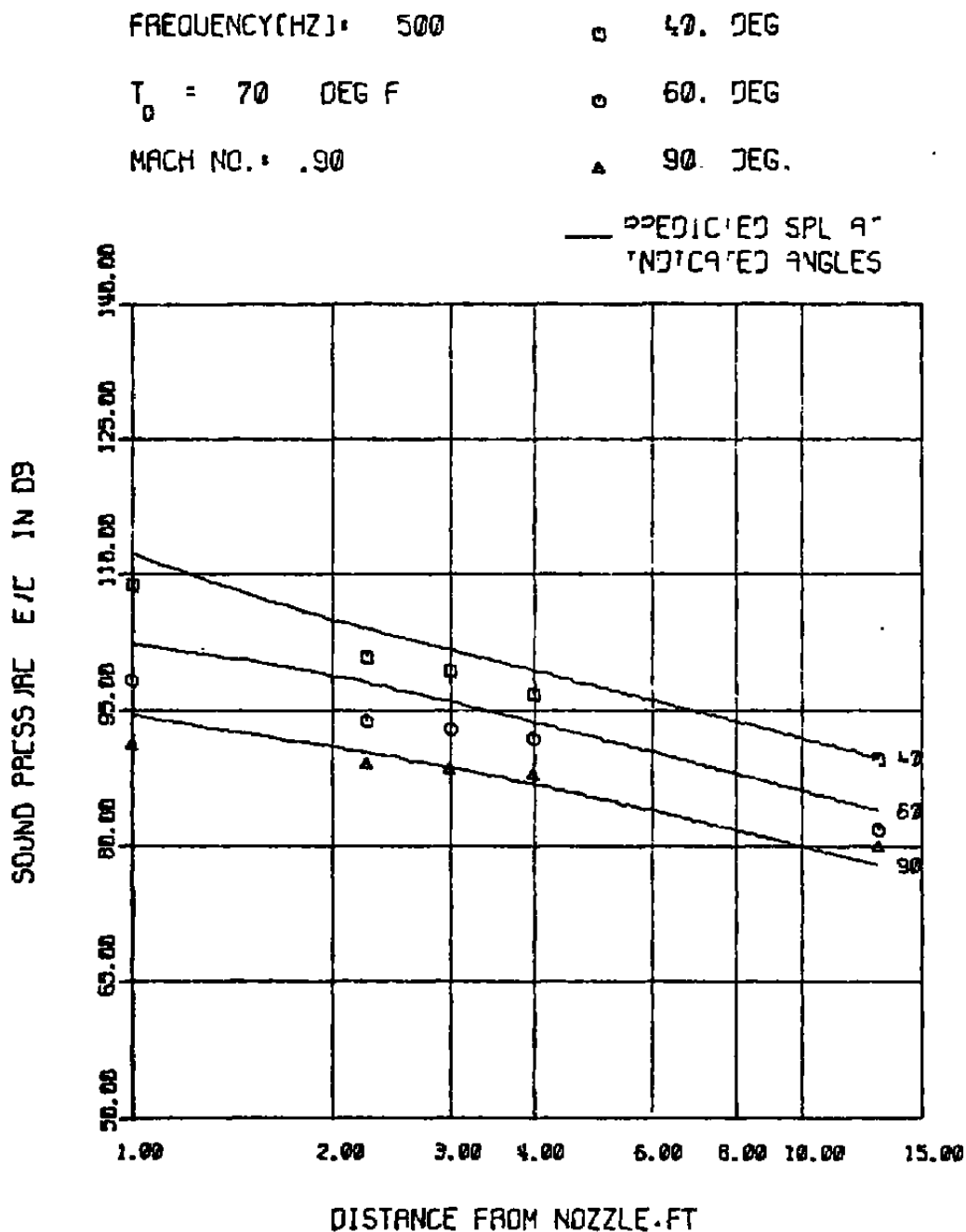
——— PREDICTED SPL AT
        INDICATED ANGLES

Fig. 28. Comparison of Measured and Predicted Sound Pressure Levels using
Modified Source Modeling Technique for Test Condition 1 at 1000 Hz.

FREQUENCY(HZ): 2000   ▢ 40. DEG.

T_0 = 80 DEG F   ◉ 60. DEG.

MACH NO.: .70   ▲ 90. DEG.

⎯⎯ PREDICTED SPL AT
INDICATED ANGLES

Fig. 29. Comparison of Measured and Predicted Sound Pressure Levels using
Modified Source Modeling Technique for Test Condition 1 at 2000 Hz.
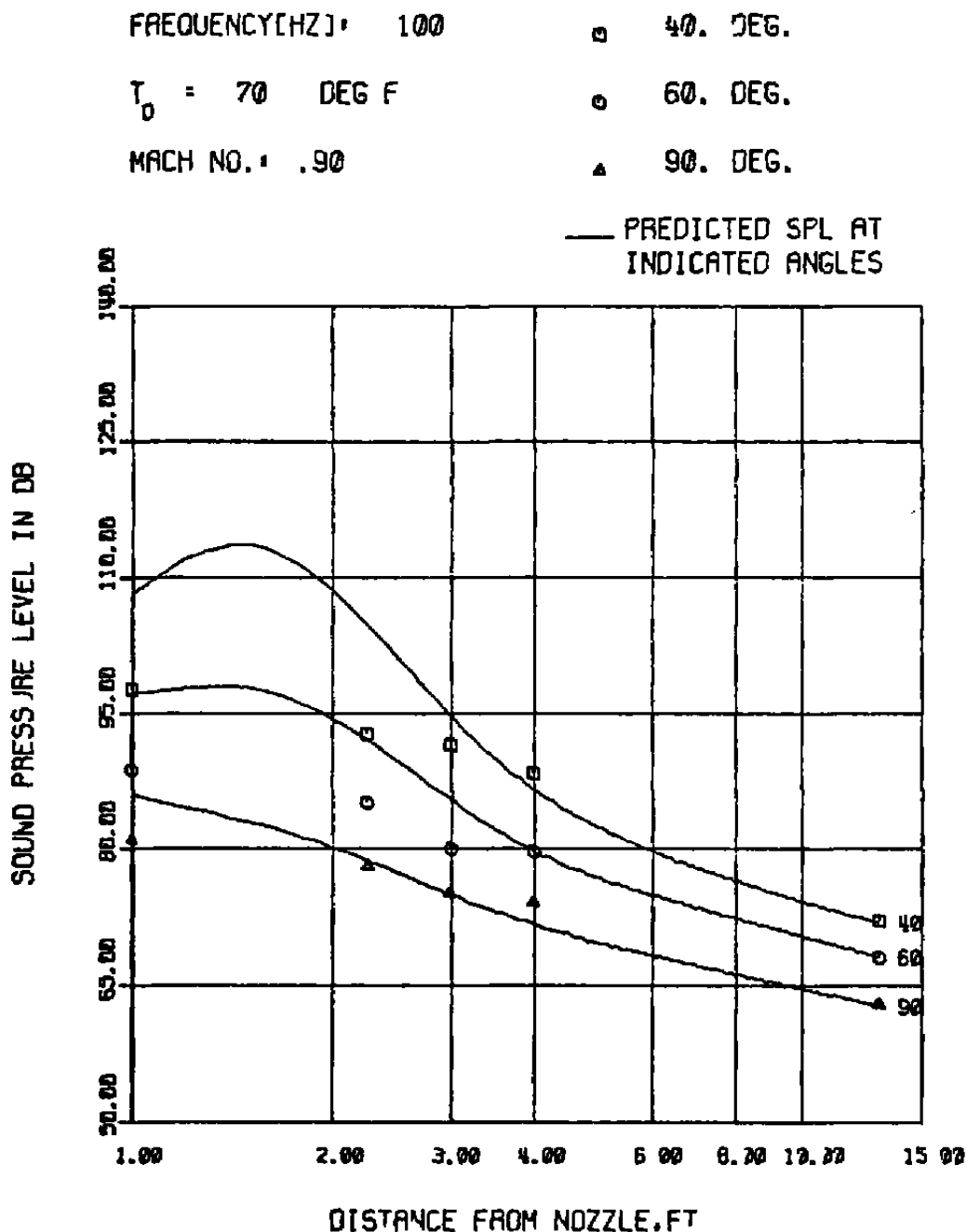
Fig. 30. Comparison of Measured and Predicted Sound Pressure Levels using
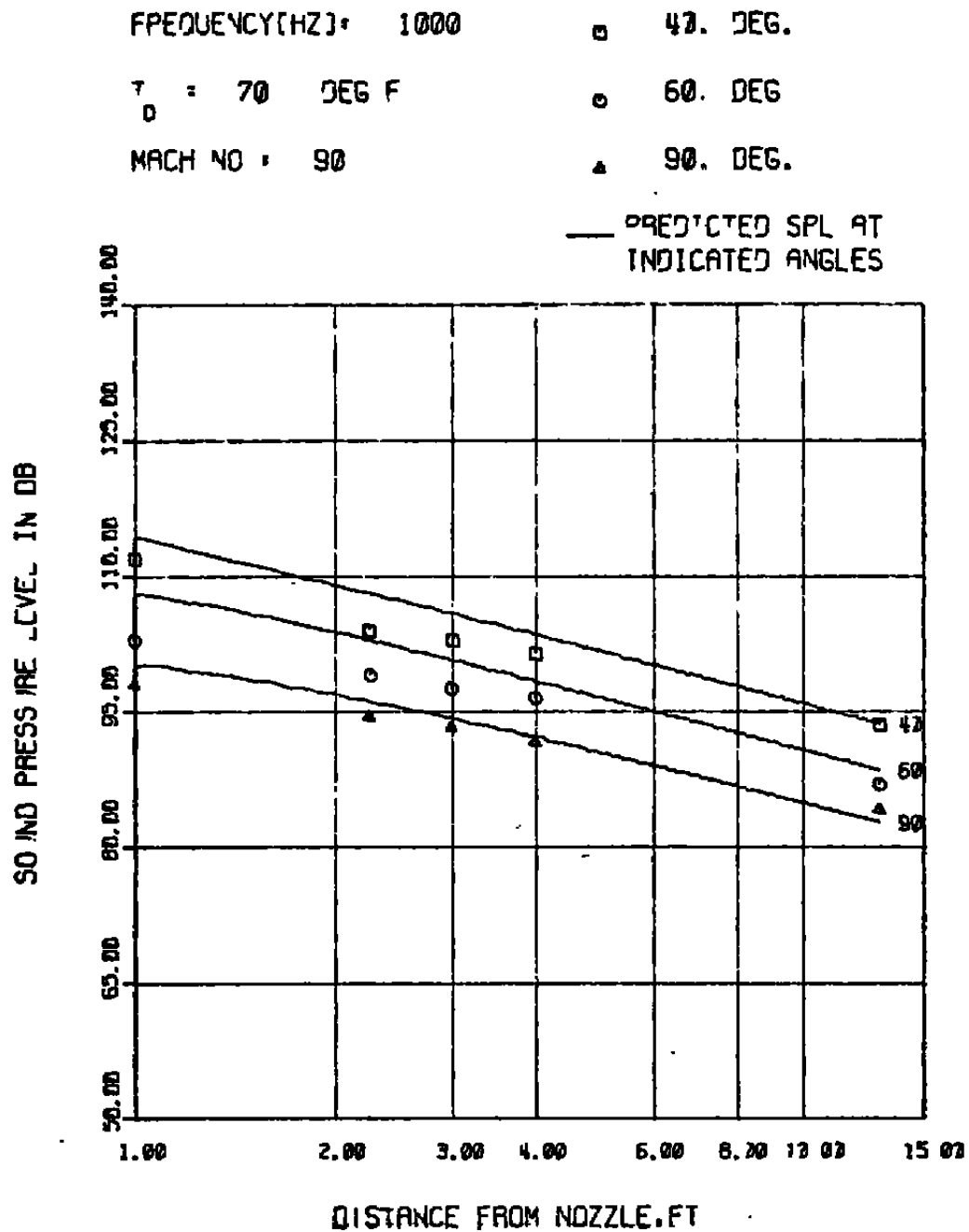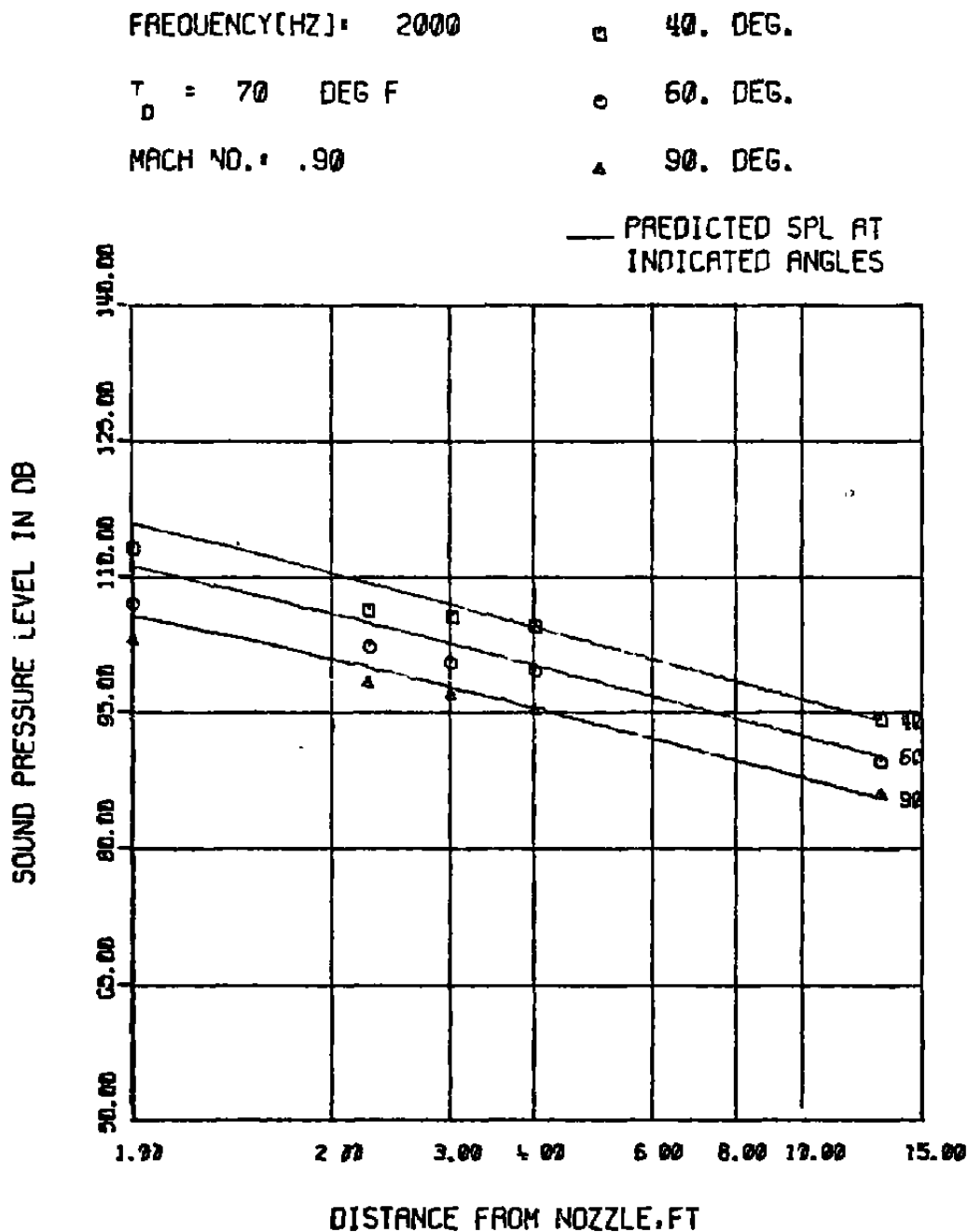Modified Source Modeling Technique for Test Condition 2 at 100 Hz.
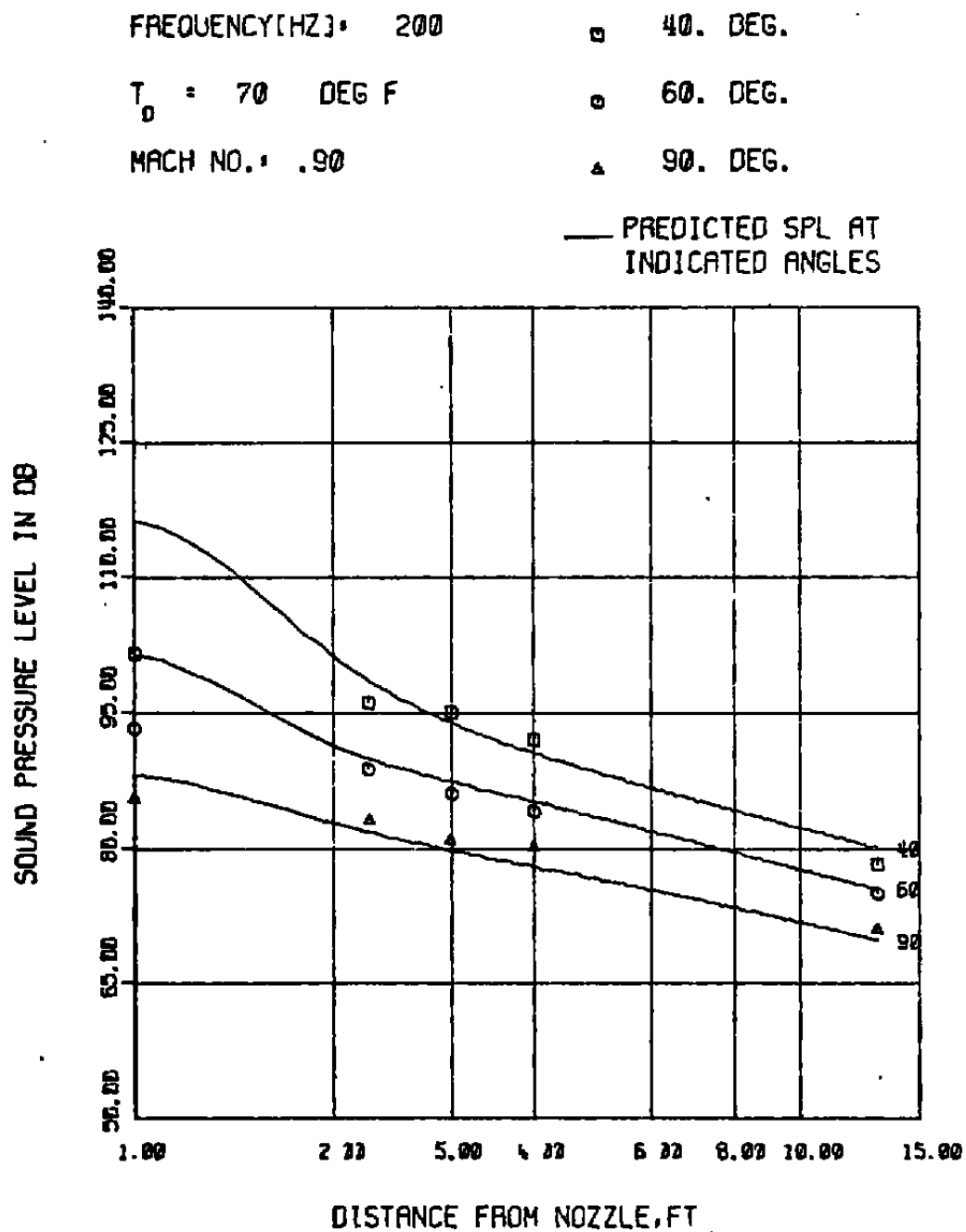
Fig. 31. Comparison of Measured and Predicted Sound Pressure Levels using Modified Source Modeling Technique for Test Condition 2 at 200 Hz.

Fig. 32. Comparison of Measured and Predicted Sound Pressure Levels using
Modified Source Modeling Technique for Test Condition 2 at 500 Hz.

Fig. 33. Comparison of Measured and Predicted Sound Pressure Levels using Modified Source Modeling Technique for Test Condition 2 at 1000 Hz.

Fig. 34. Comparison of Measured and Predicted Sound Pressure Levels using
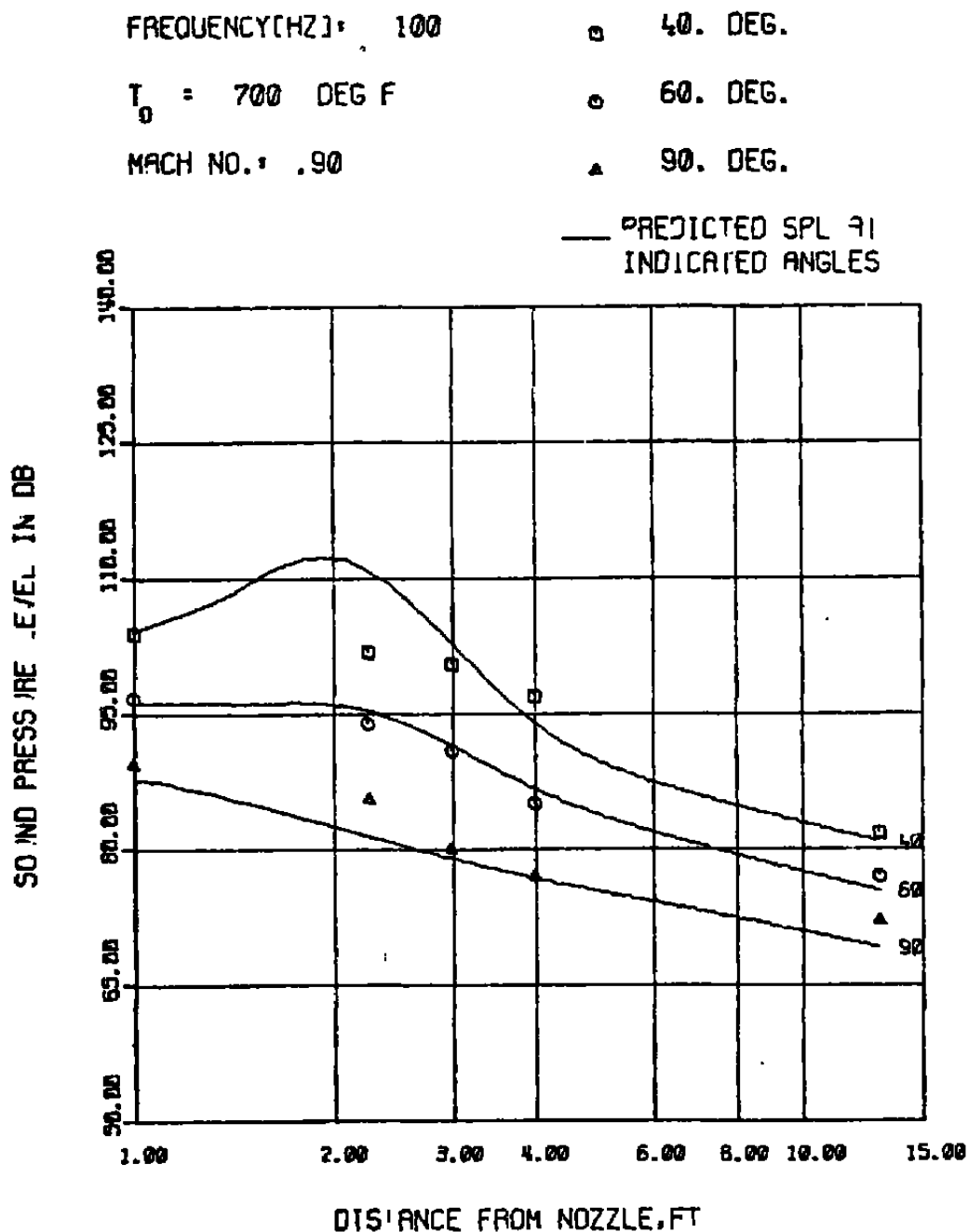Modified Source Modeling Technique for Test Condition 2 at 2000 Hz.

Fig. 35. Comparison of Measured and Predicted Sound Pressure Levels using Modified Source Modeling Technique for Test Condition 3 at 100 Hz.
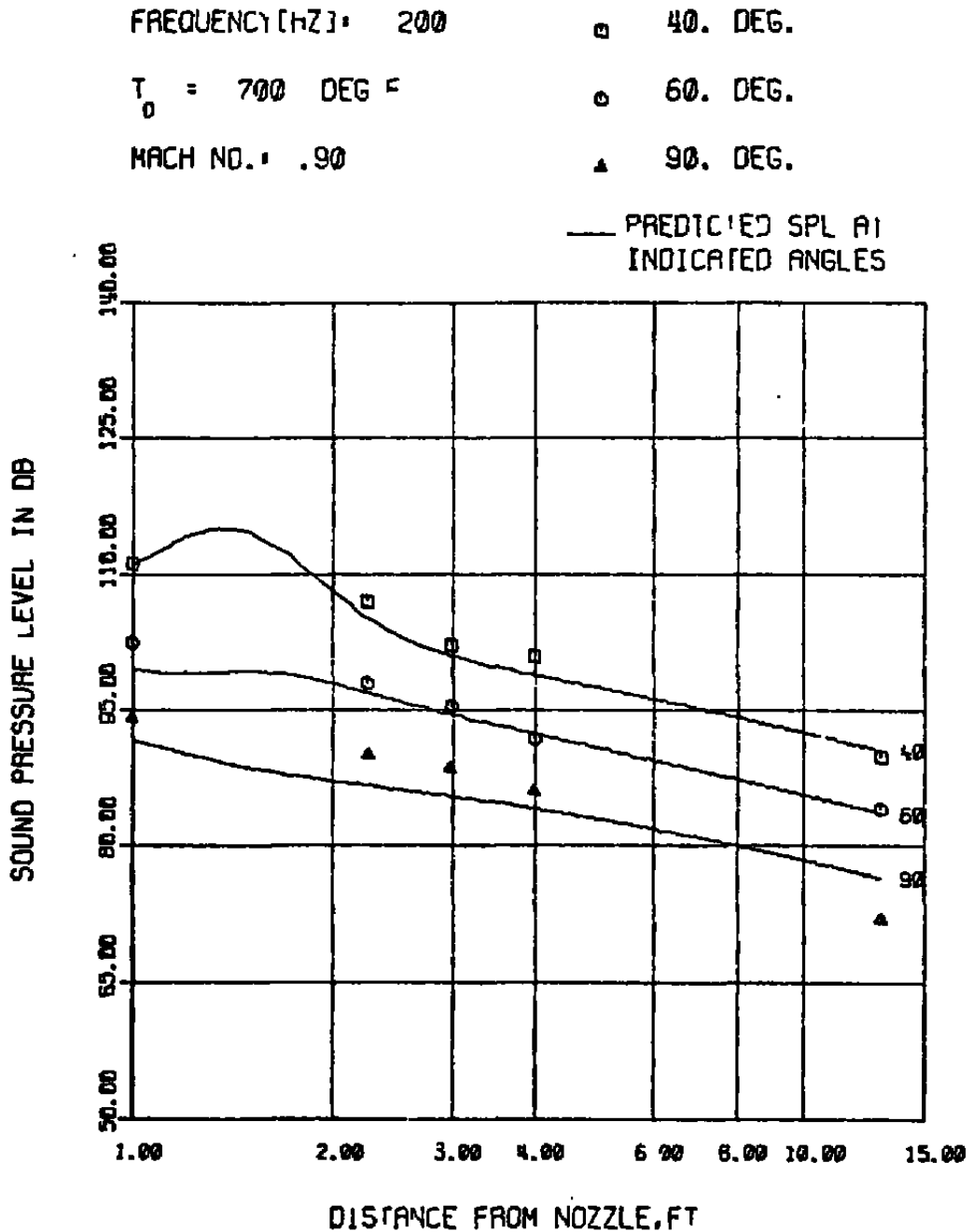
Fig. 36. Comparison of Measured and Predicted Sound Pressure Levels using Modified Source Modeling Technique for Test Condition 3 at 200 Hz.
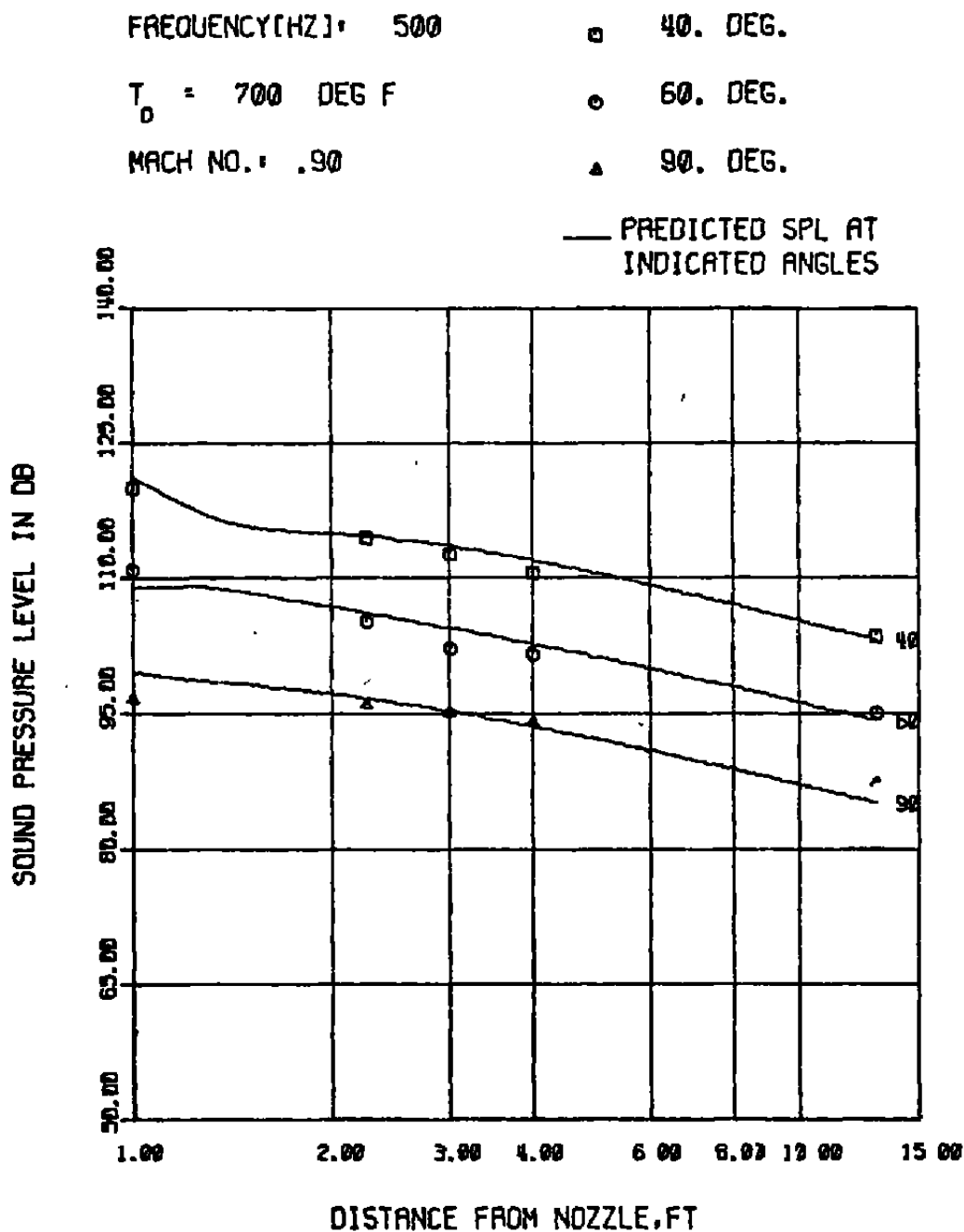
Fig. 37. Comparison of Measured and Predicted Sound Pressure Levels using Modified Source Modeling Technique for Test Condition 3 at 500 Hz.
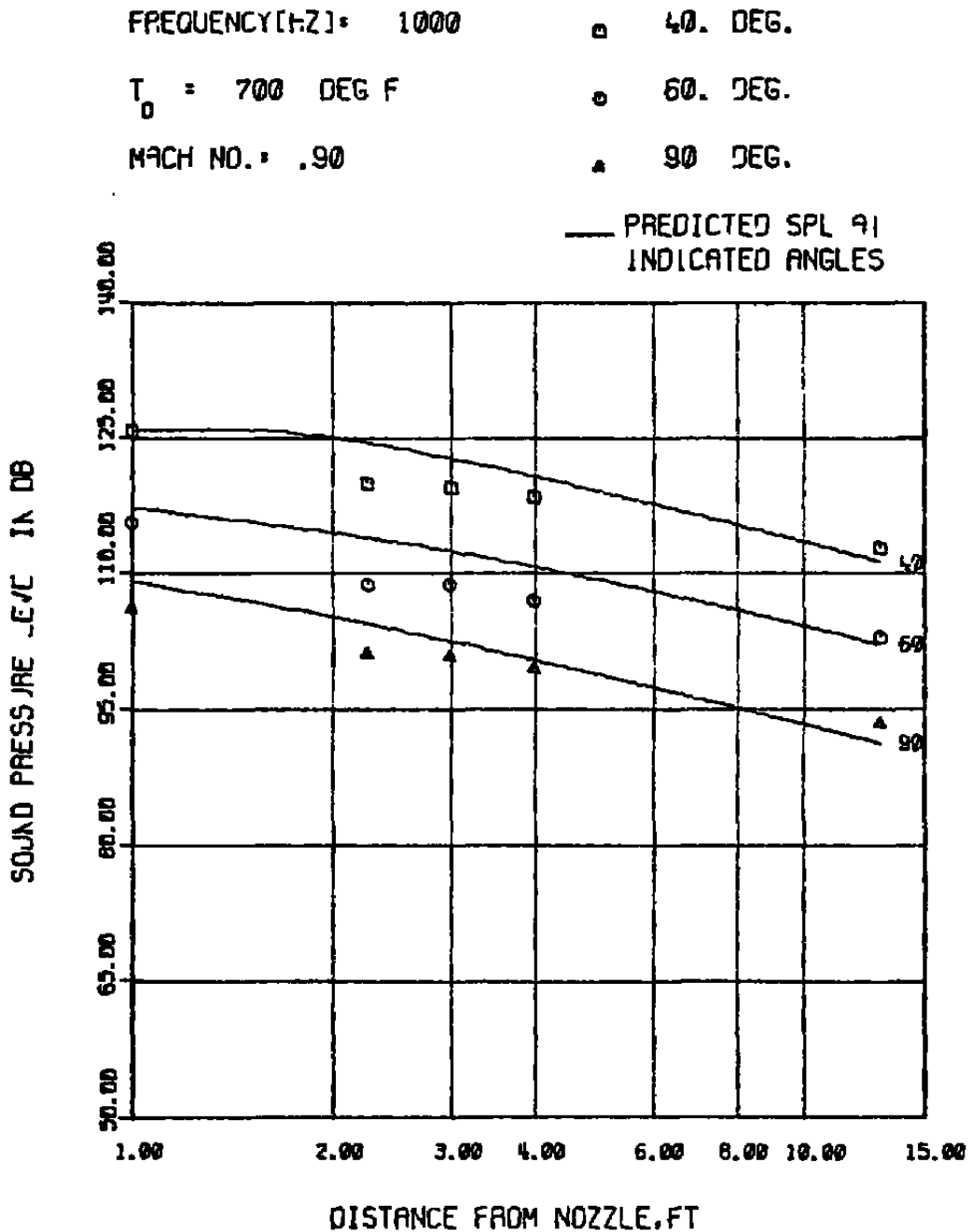
Fig. 38. Comparison of Measured and Predicted Sound Pressure Levels using Modified Source Modeling Technique for Test Condition 3 at 1000 Hz.

Fig. 39. Comparison of Measured and Predicted Sound Pressure Levels using
Modified Source Modeling Technique for Test Condition 3 at 2000 Hz.

Fig. 40. Comparison of Measured and Predicted Sound Pressure Levels using
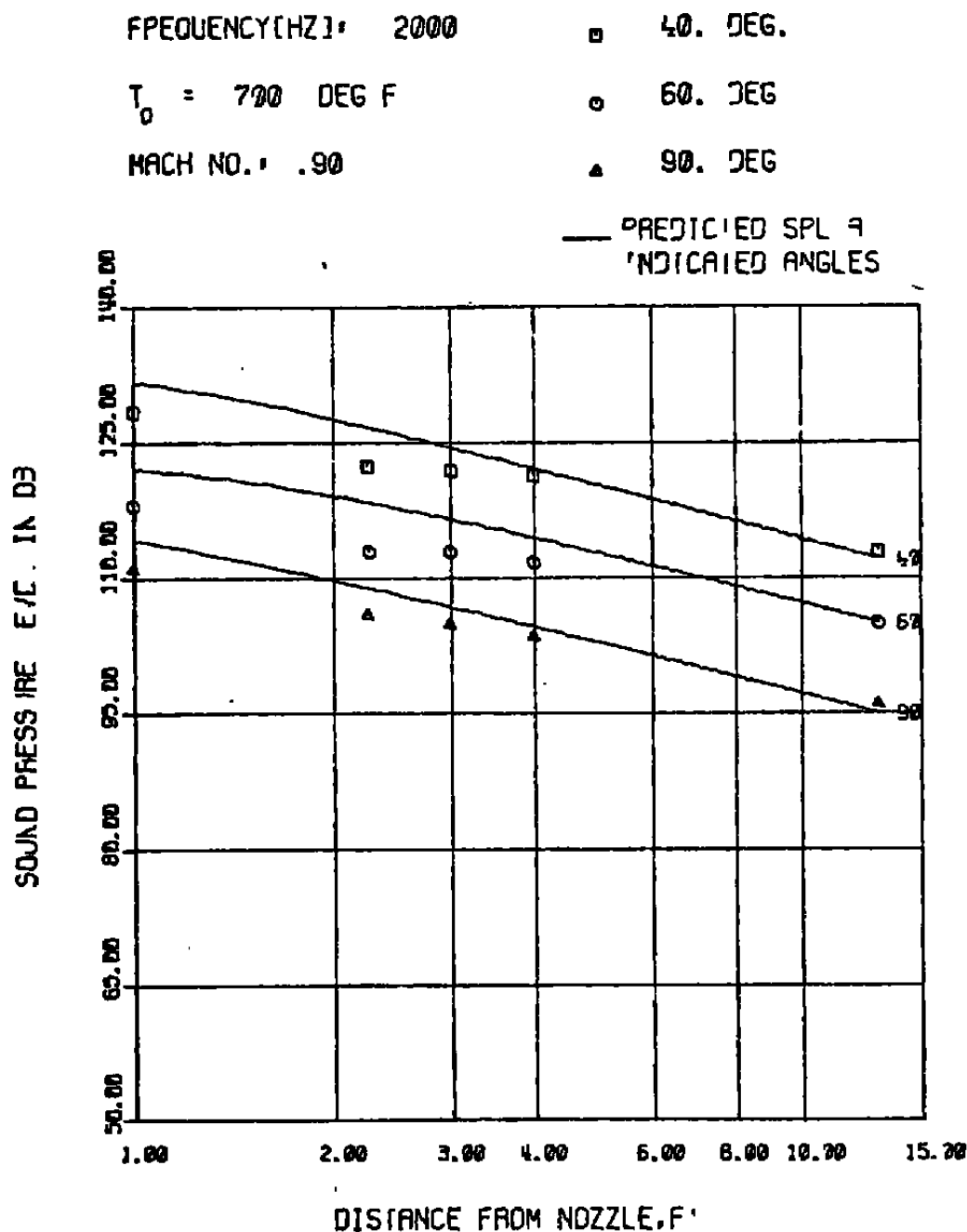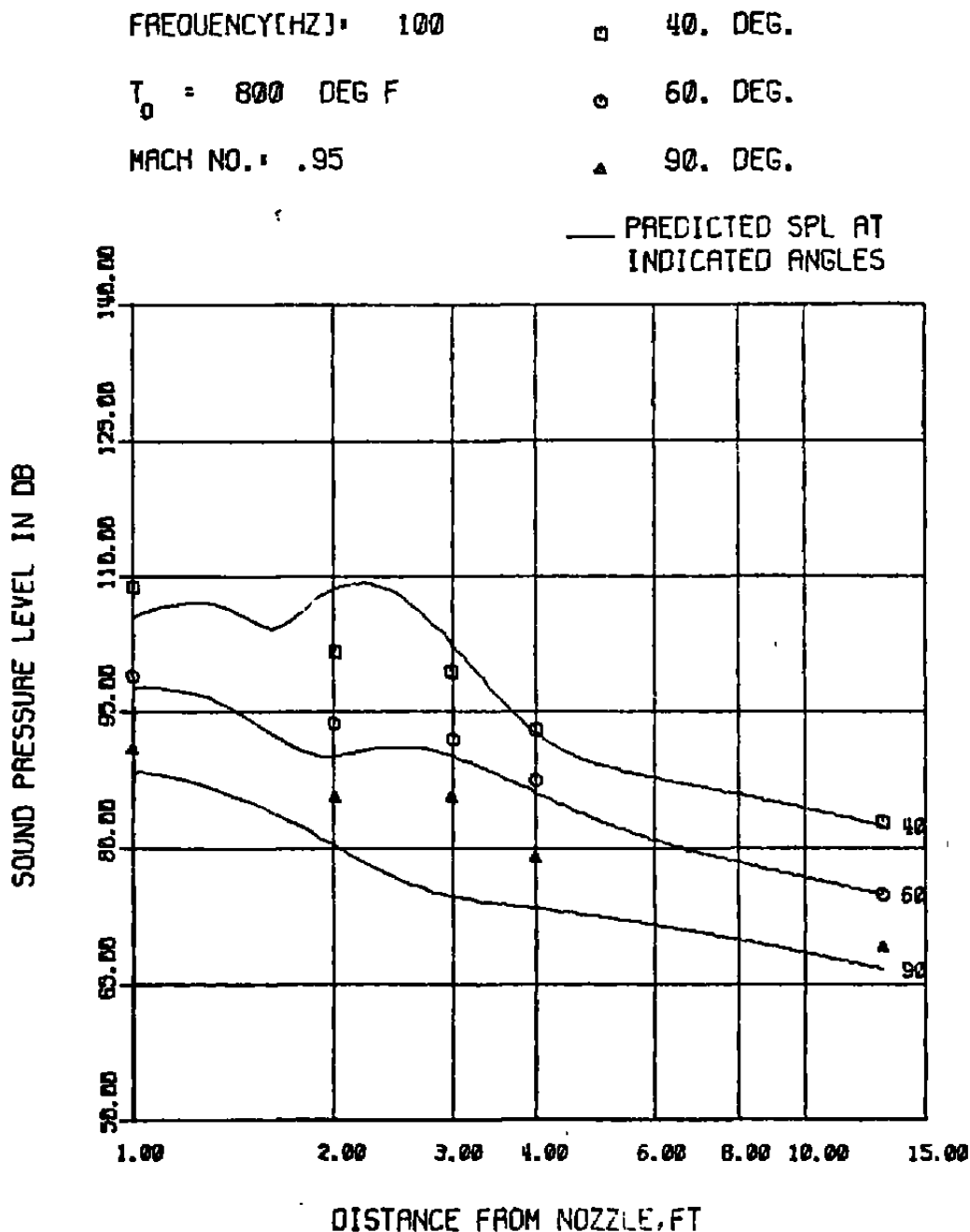Modified Source Modeling Technique for Test Condition 4 at 100 Hz.

Fig. 41. Comparison of Measured and Predicted Sound Pressure Levels using
Modified Source Modeling Technique for Test Condition 4 at 200 Hz.
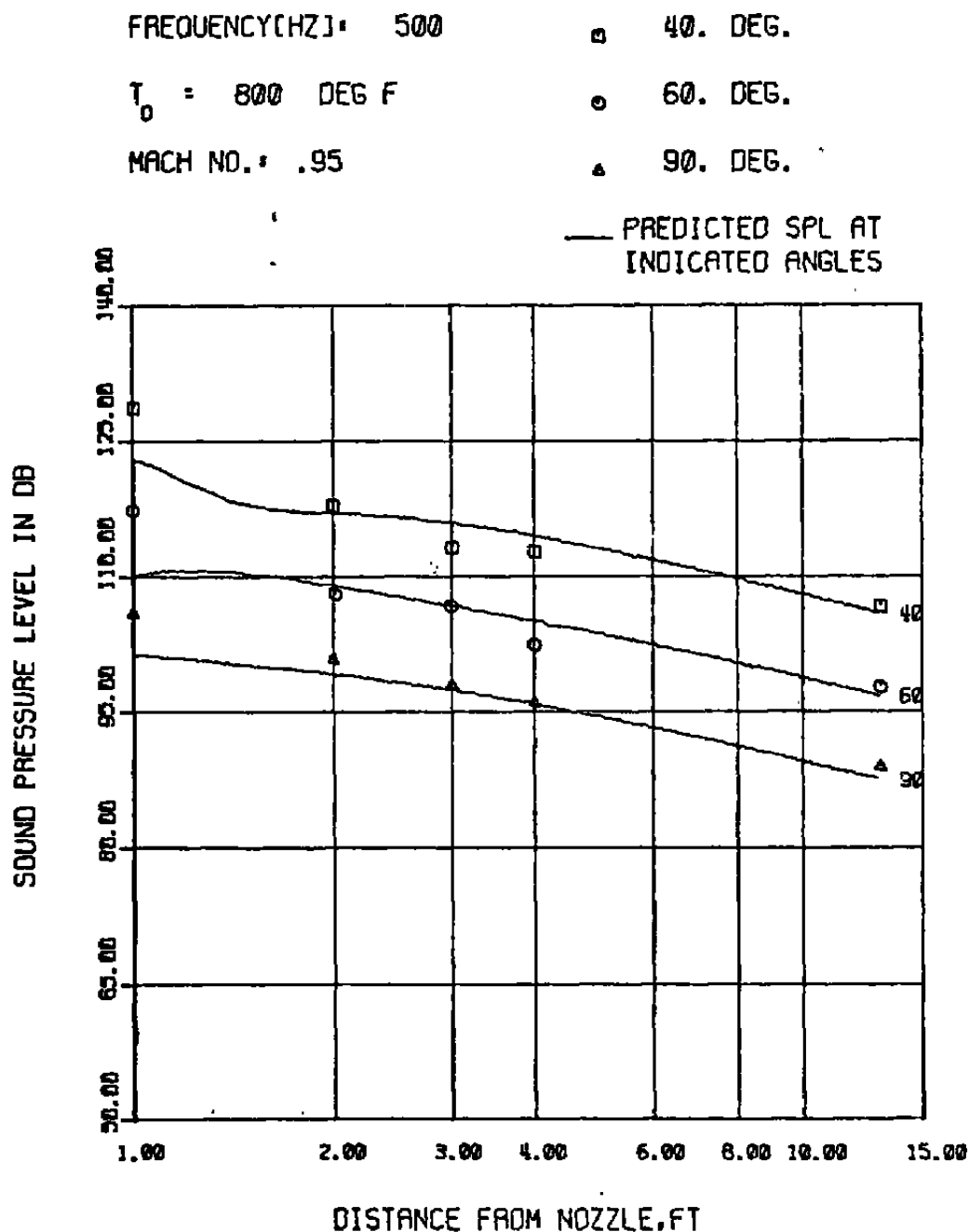
Fig. 42. Comparison of Measured and Predicted Sound Pressure Levels using Modified Source Modeling Technique for Test Condition 4 at 500 Hz.

FREQUENCY[HZ]• 1000   ▢   40. DEG.

T_0 = 800 DEG F   ⊙   60. DEG.

MACH NO.• .95   ▲   90. DEG.

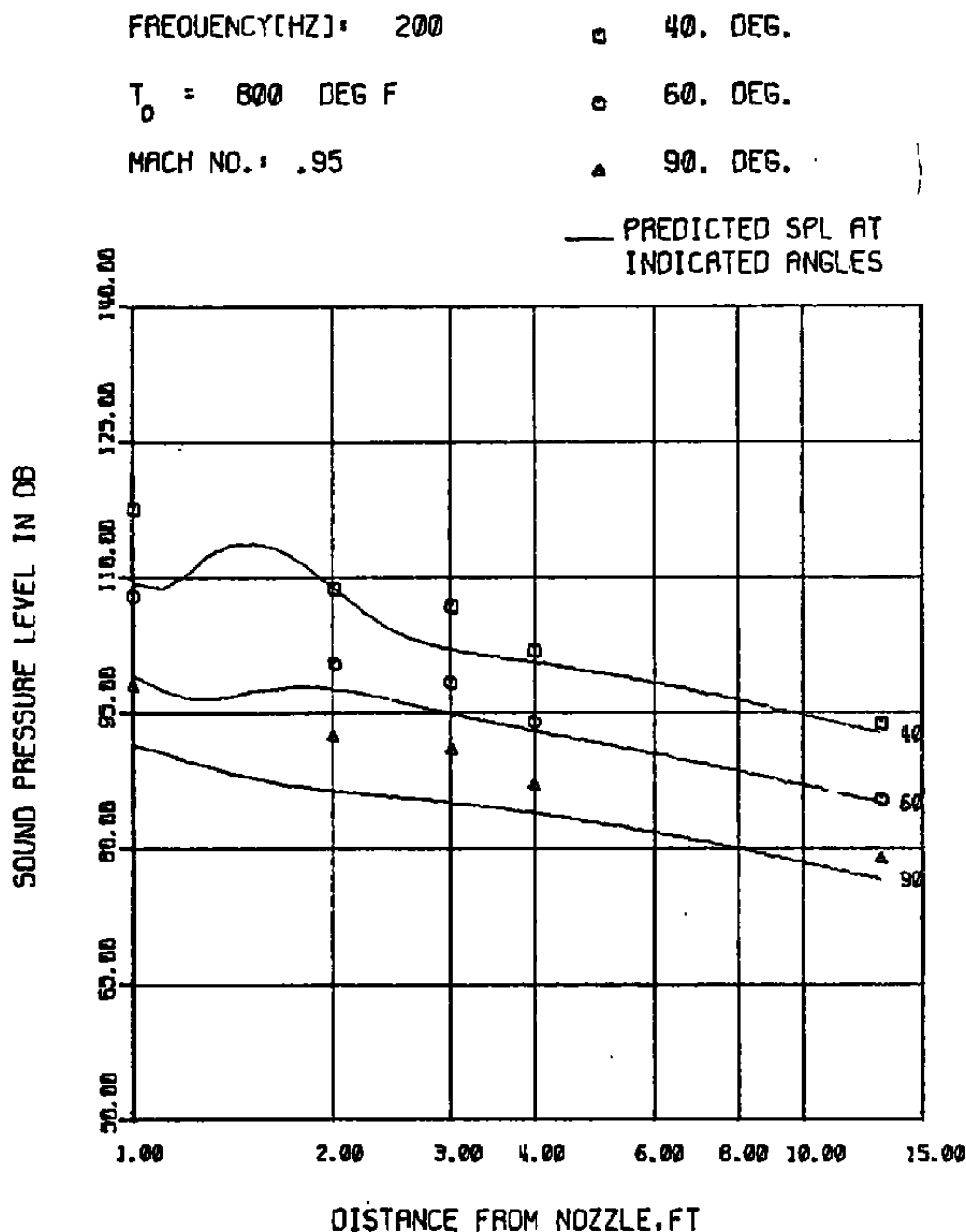___ PREDICTED SPL AT
INDICATED ANGLES

Fig. 43. Comparison of Measured and Predicted Sound Pressure Levels using Modified Source Modeling Technique for Test Condition 4 at 100 Hz.

73

Fig. 44. Comparison of Measured and Predicted Sound Pressure Levels using Modified Source Modeling Technique for Test Condition 4 at 2000 Hz.
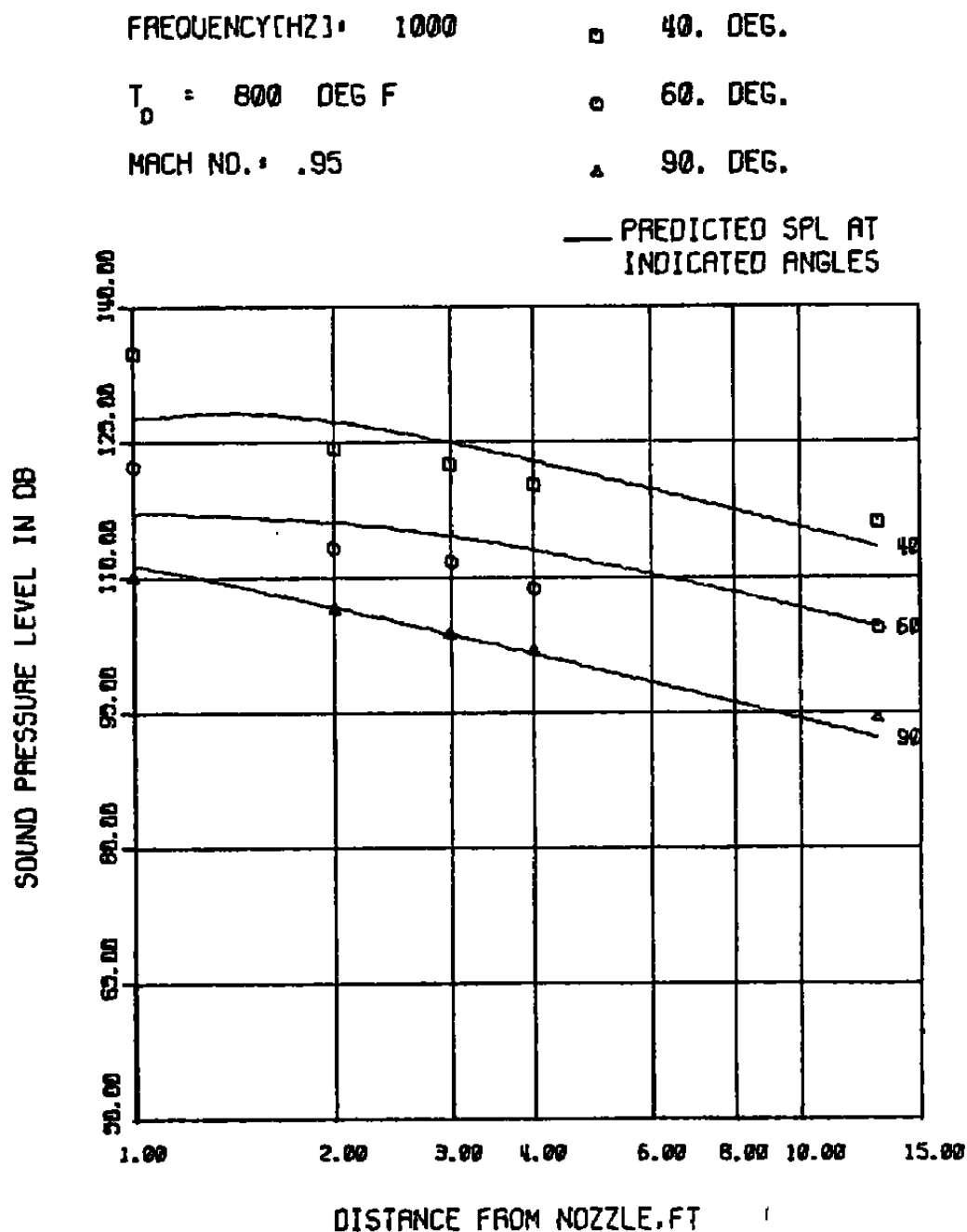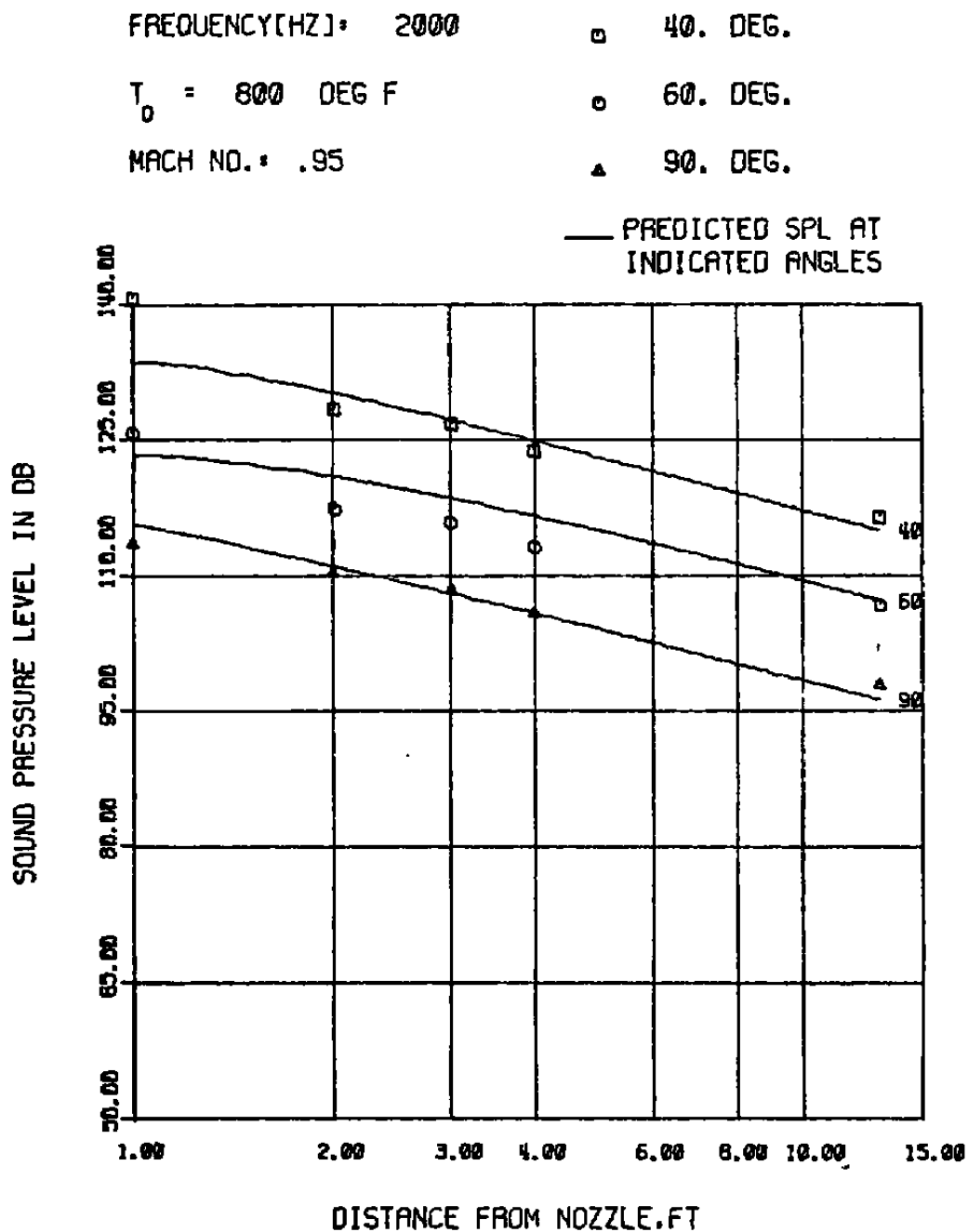
LIST OF SYMBOLS

A_1, A_2, A_3, A_4	Octupole coefficients, $k^6/M^2_{030}/(4\pi x)^2$, etc.
a_o	Ambient speed of sound
D_1, D_2	Dipole coefficient, $k^2 M^2_{100}/(4\pi x)^2$, etc.
D	Nozzle diameter
$f(x_1, x_2, x_3, t)$	Source function
f	Frequency
$f(\theta)$	Source directivity function
i	Imaginary unit, $\sqrt{-1}$
$I(x,\theta)$	Far Field intensity, $\overline{p^2}/\rho a_o$
k	Wave number, ω/a_o
M_c	Convection Mach number, V_c/a_o
$m_{jk\ell}(t)$	Multipole moment
$M_{jk\ell}$	Multipole moment amplitude
P_1	Monopole coefficient, $M^2_{000}/(4\pi x)^2$
P_o	Stagnation pressure
P_a	Ambient pressure
p	Acoustic pressure
p_m	Acoustic pressure associated with monopole terms
p_d	Acoustic pressure associated with dipole terms
p_q	Acoustic pressure associated with quadrupole terms
p_o	Acoustic pressure associated with octupole terms
Q_1, Q_2, Q_3	Quadrupole coefficients, $k^4 M^2_{200}/(4\pi x)^2$, etc.
R	Distance from source point to observation point, $\lvert \vec{x} - \vec{y} \rvert$
R_c	Convection velocity ratio, V_c/V_j
r	Radius in cylindrical coordinates
SPL	Sound pressure level, $10 \log \overline{p^2}/p^2_{ref}$

75

St	Strouhal number, fV_j/D
T_o	Stagnation temperature
V_c	Convection velocity
V_j	Jet exit velocity
x_1, x_2, x_3	Coordinates of field point
x_s	Source location
x	Distance to field point
y_1, y_2, y_3	Coordinates of source point
θ	Azimuthal angle
λ	Wavelength, a_o/f
ρ	Density
ϕ	Polar angle
ω	Frequency, $2\pi f$